Skin electroporation for transdermal drug delivery: Electrical measurements, numerical model and molecule delivery

Georgios Kougkolos, Lionel Laudebat, Sorin Dinculescu, Juliette Simon, Muriel Golzio, Zarel Valdez-Nava, Emmanuel Flahaut

Skin electroporation for transdermal drug delivery:
electrical measurements, numerical model and molecule delivery

Georgios Kougkolos[1,2], Lionel Laudebat[2,3], Sorin Dinculescu[2], Juliette Simon[1,4], Muriel Golzio[4*], Zarel Valdez-Nava[2*] and Emmanuel Flahaut[1*]

1 CIRIMAT, Université de Toulouse, CNRS, INPT, UPS, 31062 Toulouse CEDEX 9, FRANCE
2 LAPLACE, Université de Toulouse, CNRS, INPT, UPS, 31062 Toulouse CEDEX 9, France
3 INU Champollion, Université de Toulouse, 81012 Albi, France
4 IPBS, Université de Toulouse, CNRS UMR, UPS, 31077 Toulouse CEDEX 4, FRANCE
* Corresponding authors: Dr Muriel Golzio (muriel.golzio@ipbs.fr), Dr Zarel Valdez-Nava (valdez@laplace.univ-tlse.fr), Dr Emmanuel Flahaut (emmanuel.flahaut@univ-tlse3.fr)

Abstract

Skin electroporation for drug delivery involves the application of Pulsed Electric Fields (PEFs) on the skin to disrupt its barrier function in a temporary and non-invasive manner, increasing the uptake of drugs. It represents a potential alternative to delivery methods that are invasive (*e.g.* injections) or limited. We have developed a drug delivery system comprising nanocomposite hydrogels which act as a reservoir for the drug and an electrode for applying electric pulses on the skin. In this study, we employed a multi-scale approach to investigate the drug delivery system on a mouse skin model, through electrical measurements, numerical modeling and fluorescence microscopy. The Electrical properties indicated a highly non-linear skin conductivity behavior and were used to fine-tune the simulations and study skin recovery after electroporation. Simulation of electric field distribution in the skin showed amplitudes in the range of reversible tissue electroporation (400-1200 V/cm), for 300 V PEF. Fluorescence microscopy revealed increased uptake of fluorescent molecules compared to the non-pulsed control. We reported two reversible electroporation domains for our configuration: (1) at 100 V PEF the first local transport regions appear in the extracellular lipids of the stratum corneum, demonstrated by a rapid increase in the skin's conductivity and an increased uptake of lucifer yellow, a small hydrophilic fluorophore and (2) at 300 V PEF, the first permeabilization of nucleated cells occurred, evidenced by the increased fluorescence of propidium iodide, a membrane-impermeable, DNA intercalating agent.

Keywords: Skin electroporation, Drug delivery, Hydrogel, FEM simulation, Electrical properties, Stratum corneum
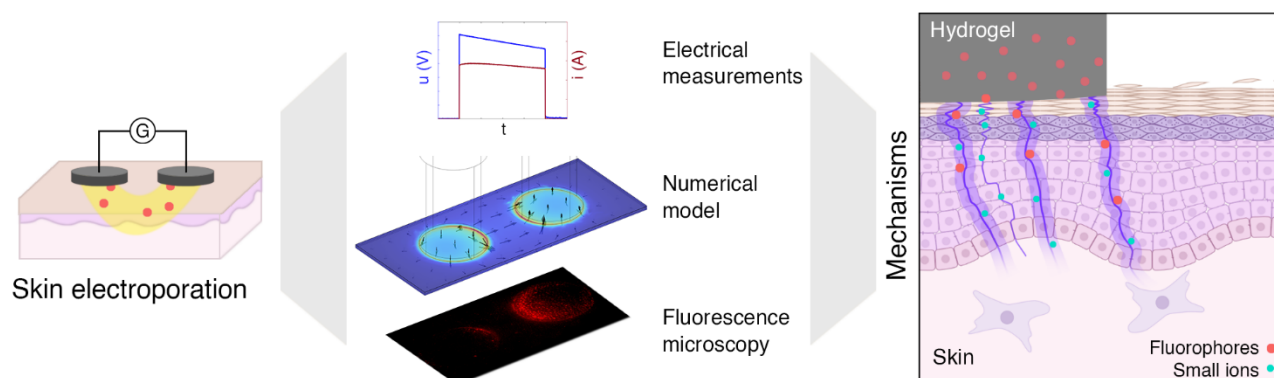
Fig. 0. Graphical abstract. Skin electroporation for transdermal drug delivery assessed by electrical measurements, numerical modeling and delivery of fluorescent molecules.

Highlights

- Nanocomposite hydrogels function as drug reservoirs and electrodes
- Integrated electrical measurements, numerical modeling & molecule delivery
- Skin resistance drops with electric field strength
- Stratum corneum barrier disruption at 100 V
- Cell membrane permeabilization at 300 V in viable skin

1. Introduction

The skin represents an accessible and convenient route for non-invasive drug delivery. Medicine administered through the skin avoids the first-pass metabolism and the gastrointestinal tract [1]. Transdermal delivery platforms, such as nicotine patches, can effectively administer drugs through the epidermis in a controlled manner. Advantages include increased bioavailability, sustained steady-state blood concentration levels, painless self-administration and reduced frequency of dosing, which in turn improve patient compliance and quality of life [2]. However, the skin, and more specifically its outermost layer, the stratum corneum (SC), acts as a barrier protecting the organism from the penetration of exogenous substances and microbes and limiting water loss. Passive diffusion of drugs through the skin is only achieved for low molecular weight (MW<400-500 Da), relatively lipophilic molecules (log$P$ around 2 to 3) [3]. Several chemical and physical methods are being developed, allowing bigger and/or hydrophilic molecules to cross the skin barrier. Among these, skin electroporation consists in applying electric field pulses with high voltage (50 to 3000 V) and short duration (5 µs to 100 ms) on the surface of the skin, permeabilizing the SC in a non-invasive and temporary manner [4]–[6].

In humans (and most mammals), the skin can be divided into three layers: the epidermis, the dermis and the hypodermis. The epidermis is a stratified epithelium consisting mainly of keratinocytes. These cells proliferate in the basal layer of the epidermis and progressively migrate outwards while terminally differentiating, forming the spinous layer, the granular layer and the stratum corneum (or cornified layer) [7]. The keratinocytes of the SC are 15-20 layers of flattened, dead cells with a cornified envelope replacing their plasma membrane, and they form the layer responsible for the barrier function of the skin. The extracellular space in the SC is occupied by lipids (ceramides, fatty acids, cholesterol and cholesterol esters) that are attached to the cornified envelope and are largely organized in stacks of lipid bilayers [8], [9]. The dermis is a layer of connective tissue with collagen, fibroblasts and high water content that provides nutrients to the epidermis and protects the organism against mechanical injury [7]. Both the dermis and the epidermis are also traversed by skin appendages, notably hair follicles, sebaceous glands and eccrine glands [10]. The subcutaneous tissue (or hypodermis) is located below the dermis. It is composed of loose connective tissue, including collagen and elastin fibers, as well as adipose tissue. The dermis and the hypodermis have a rich blood supply, provided by a highly branched network of blood vessels [10].

Electroporation is a bioelectrical phenomenon where a lipid bilayer is permeabilized through the application of an external electric field [11], [12]. Depending on the parameters of the electric field (strength, duration, waveform, number and frequency of repetitions in the case of PEF) and the electrode configuration, the permeabilization may be transient (reversible EP) or permanent (irreversible EP). Reversible electroporation has found numerous applications most notably in biotechnology, for inserting genes into cells (gene electro-transfer) [13] and for fusing cells (electrofusion) *in vitro* [14]; in medical applications for cancer treatment, through the uptake of membrane-impermeant drugs into cancer cells [15]; and in drug delivery through the needle-free

transport of molecules across the epidermis [2] or drug and nucleic acid administration through injection of the agents (drugs, vaccines) into tissue, followed by PEF application [16], [17].

Skin electroporation for non-invasive, transdermal drug delivery was first suggested by Prausnitz *et al.* in 1993. They demonstrated that the application of PEF on human skin*, ex vivo*, and hairless mouse skin, *in vivo*, lead to a temporary, multi-fold increase on the uptake of three small to medium-sized, negatively charged, fluorescent molecules (lucifer yellow, calcein, erythrosin derivative), compared to a non-pulsed control [9]. Since then, numerous studies have been published on skin electroporation for transdermal drug delivery, expanding the results to a wider range of molecules (charge and size) and testing different electrode configurations and pulse parameters, on a variety of skin models (mouse, pig, reconstructed human, human) [2], [18]–[25]. However, very few studies have reached human *in vivo* testing of this delivery method [26], [27]. A number of limitations prevent transdermal electroporation for drug delivery from reaching clinical trials. These include inconsistent drug delivery quantities, unpractical electrode configurations, unclear pain thresholds for PEFs, failure to deliver larger molecules and a general limited understanding of the underlying mechanisms. A successful non-invasive transdermal drug delivery has to be painless, practical, totally-reversible and must deliver consistent amounts of therapeutic molecules in relevant quantities, within reasonable timeframes.

The critical parameter in lipid bilayer electroporation is the electric potential difference across the bilayer. The application of an external electric field charges the bilayer, which has dielectric properties, up to a critical threshold, when electroporation is observed. For plasma membranes, this threshold is experimentally calculated to be approx. 250 mV, in eukaryotic cells [28]. Electroporation is observed through the loss of the barrier properties of the bilayer (transport of water and solutes through it) and a rapid potential decrease across it. While the exact mechanism of electroporation at the molecular level is not fully elucidated, it is proposed that it may be caused by structural rearrangement of the lipids, forming aqueous pores, electrically-induced chemical modifications of the lipid chains or a combination of these [12]. Molecular dynamics simulations of lipid bilayers under strong electric fields have pointed out towards the formation of short-lived aqueous pores [29]. On a tissue level, an electric field higher than 400 V/cm can permeabilize the plasma membranes of cells within the tissue [30]. Starting at approx. 1200 V/cm and over, the PEF application may induce permanent permeabilization and cell death, *i.e.* the electroporation is irreversible [30].

At the skin level, the application of an external electric field can disrupt the barrier function of the SC by creating Local Transport Regions (LTRs), *i.e.* aqueous pathways through the skin [30], [31]. LTRs are regions of increased ionic mobility and increased solute mass transfer, with enhanced electrical conductivity and permeability. Their appearance is accompanied by a rapid decrease in the resistivity of the SC (up to three orders of magnitude [32]), increase in transepidermal water loss, and increased permeability to hydrophilic compounds [6], [24]. The high current density that circulates through LTRs causes Joule heating and melting of the lipids in their vicinity, further increasing their size for longer pulse durations. Higher applied voltages increase the density of LTRs and longer durations (pulse duration and number of repetitions) increase their diameter [2], [31]. For certain electrical parameters, with voltage being the most important, these changes are mostly or fully reversible. Recently, Gupta and Rai visualized the pore formation on the extracellular lipid bilayers of the SC through molecular dynamics simulations [33].

Once LTRs are formed, drug delivery across the skin can take place. The driving forces for the mass transfer of solutes are (1) electrophoretic drag (for charged entities), (2) electro-osmosis and (3) concentration gradient [2]. In the case of skin electroporation for drug delivery, three pathways through the SC are possible: (1) the paracellular pathway, a tortuous pathway through the extracellular lipids of the SC; (2) the transcellular pathway, a more direct pathway through the corneocytes (implies

permeabilization of their cornified envelopes), and (3) the transappendegeal pathway, following the hair follicles or the sweat ducts of the SC [18], [34]. Transport of molecules may include a combination of these pathways but the paracellular is generally accepted as the dominant one [2], [24], [33].

Several factors, both physical and chemical in nature —such as temperature, pH, and chemical enhancers— have an impact on skin permeability. These methods can be utilized in conjunction with skin electroporation to enhance its effectiveness. Their action mechanism can be categorized into three types, either independently or in combination: (1) reducing the electric field threshold required for forming Local Transport Regions (LTRs), (2) increasing the size of LTRs, and (3) extending the duration of LTRs. Moderately increased skin temperatures (40 to 45 °C), coupled with PEF application, increase the transport of molecules through the SC [35] and cell permeabilization [36]. Neutral and alkaline pH impedes the barrier function recovery of the skin, prolonging the duration of LTRs [37], [38]. Surfactants (Sodium dodecyl sulfate [39]), anionic lipids (mixture of 1,2-dioleoyl-3-phosphatidylglycerol and 1,2-dioleoyl-3-phosphatidylcholine [40], 1,2-dimyristoyl-3-phosphatidylserine [41]), reducing agents (thiosulfate [42]) and charged macromolecules (heparin [43], [44], dextran sulfate [44]) can be used to increase transdermal transport, in parallel with electroporation. These chemical enhancers have different proposed mechanisms. Surfactants interfere with the lipid bilayers of the SC. Combined with the application of a PEF, they facilitate barrier disruption and prolong the formed LTRs [39]. Anionic lipids and macromolecules stabilize the formed pathways and prolong their duration [40], [43], [44]. Reducing agents break the disulfide bonds of the corneocyte keratin matrix, enlarging the LTRs [42].

In the current work we chose to not include physical and chemical permeability enhancers, in order to study the interaction of increasing PEF voltages with the mouse skin. However, the application of an electric field on the tissue engenders some physical and chemical changes which can affect permeabilization such as temperature increase due to joule heating and pH changes due to water electrolysis. These are discussed in the results and discussion section.

The most common electrode configurations for skin electroporation are presented in **Fig. 1**. These include the two-chamber configuration [9], the skinfold configuration [45] and our configuration [46], two-in-one electrode-reservoir hydrogels, placed side by side. Some less common configurations include two cylindrical L-shaped electrodes side by side [47], multi-electrode arrays [48] and meander electrodes [49]. In general, the configurations include one (or more) positive electrode(s), one (or more) negative electrode(s), the model skin, the drug/model molecule formulation and (optionally) a conductive material to facilitate contact between the skin model and the electrodes. Some of these components may be combined.
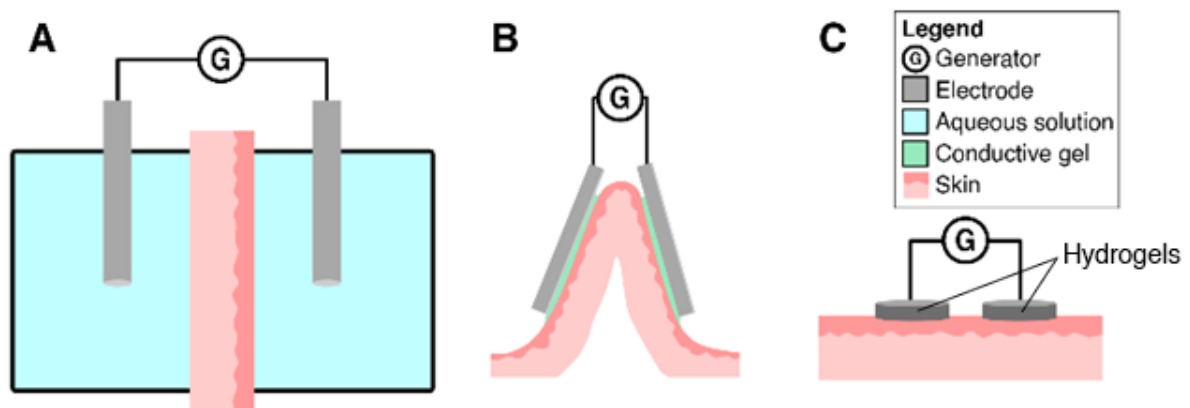
Fig. 1. Configurations for skin electroporation. **(A)** Two-chamber [9]. An *ex vivo* skin model is placed between two chambers, filled with an aqueous solution. The electrodes are immersed in the solutions. This configuration is only relevant for research purposes. **(B)** Pinched skin with conductive gel [45]. The skin model (*ex vivo* or *in vivo*) is pinched and placed between two electrodes. A Conductive gel placed between the metal electrodes and the skinfold ensures electrical contact. **(C)** Our configuration [46]. Side by side hydrogels functioning as drug reservoirs and electrodes.

We have developed a conductive nanocomposite hydrogel that functions both as a reservoir for a drug and an electrode for the application of electrical pulses to the skin (**Fig. 1C**), by incorporating conductive Carbon Nanotubes (CNTs) into a hydrophilic and biocompatible agarose polymer matrix. Electrically conductive, nanocomposite hydrogels are widely used in controlled drug delivery, due to their hydrophilicity, biocompatibility, retention capacity and potential responsiveness to stimuli [50]. Our configuration is efficient and practical, avoiding altogether problems arising from skin pinching, and the use of conductive gels and different drug formulations. Previously, we studied the absorption and release kinetics of the nanocomposite hydrogels [46], measured their electrical properties [51] and demonstrated the transdermal delivery of model molecules using fluorescence microscopy on histological tissue sections of mouse skin [23]. The drug delivery was found to depend on the charge and size of the model molecule and the disruption of the skin's barrier function was reversible for PEFs of 300 V [23]. In the current work, we expanded our results with real-time electrical measurements during electroporation and numerical modeling of the system coupled with fluorescent molecule delivery for validation. First, we applied PEFs and measured the skin's resistance before, during and after the application of the pulses. Then, we used these results to adjust a numerical model of the system. Finally, we compared the model with transdermal delivery of fluorescent molecules and discussed on the mechanisms of skin electroporation. Employing fluorophores with different properties, we determined distinctly the threshold for disruption of the skin barrier function through the formation of LTRs in the extracellular lipids of the SC, and the threshold for permeabilization of the plasma membranes of viable cells in the epidermis and dermis.

2. Materials and methods

2.1 Skin models

The electroporation experiments were conducted on freshly-extracted, dorsal mouse skin. Two mice strains were used: female hairless SKH1 mice (Charles River, France) aged 8 to 16 weeks and weighing between 25 and 35 g, and male and female C57BL/6 mice, aged 8 to 16 weeks and weighing 20 to 30 g. With the latter, hair removal was performed two days before using a depilatory cream (Veet). The explanted mice skin had a thickness of 0.46 ± 0.07 mm. They were cut into rectangles with average dimensions (14 ± 1) x (33 ± 4) mm, for the electroporation experiments. All experiments were performed 15 minutes to 2 hours after mice euthanasia and skin extraction.

2.2 Nanocomposite hydrogels

The nanocomposite hydrogels were prepared as previously described, but with an increased concentration of CNTs [46]. Briefly, 1.25 g of agarose (Sigma-Aldrich, CAS: 9012-36-6) were dissolved into 25 ml of deionized water at 90 °C, under magnetic stirring, while 125 mg of lab-produced double-wall CNTs were suspended into another 25 ml of deionized water through 1 hour of probe sonication (Vibra Cell, Bioblock scientific, 12 mm diameter, 1 s ON/1 s OFF, 30 % amplitude, 750 W max power) and with the addition of 12.5 mg of carboxymethyl cellulose (Fluka, CAS: 9004-32-4), used as a dispersant. The agarose solution and CNT suspension were then mixed together through 20 min of dispersion with a mini disperser (IKA ultra-turrax T10, 8000 rpm) and magnetic stirring, before being cast into silicone molds of 10 mm diameter and 2 mm height, and left to cool down for 5-10 min at room temperature. The resulting nanocomposite hydrogels were then dried (48 h, 30 °C, between two metal plates) and stored till use. Prior to use, the dry hydrogels were immersed for 24 h in electroporation buffer solution (8.1 mM K_2HPO_4, 1.9 mM KH_2PO_4, 1 mM $MgCl$, 250 mM saccharose; σ=0.15 S/m, pH=7.4) with one or two types of fluorescent molecules. The fluorescent molecules used were Lucifer Yellow (LY, Sigma-Aldrich, CAS: 67769-47-5), at a concentration of 1 mM, Propidium Iodide (PI, Sigma-Aldrich, CAS: 25535-16-4) at a concentration of 0.1 mM, and Fluorescein isothiocyanate–dextran of average molecular weight 4 kDa (FD4, Sigma-Aldrich, CAS: 60842-46-8) at a concentration of 1 mM.

2.3 *In situ* electrical measurements

Freshly-extracted mouse skin was placed on a gauze soaked with commercial phosphate buffer saline (PBS without Ca^{2+} and Mg^{2+}, Eurobio Scientific), inside a plastic petri dish. An electrical heater under the petri dish kept the temperature of the skin at 32 °C, corresponding to the skin surface temperature of the human forearm [52]. Two hydrogel electrodes were placed on the surface of the skin, 14 mm apart (center-to-center). Stainless steel cylindrical electrical contacts were placed on top of each hydrogel and were connected to an electrical generator (ELECTRO cell B10 HVLV, Betatech). The PEF applied consisted of 8 square unipolar pulses of 20 ms duration, frequency of 1 Hz and voltage of 0 (control) to 400 V. The potential difference and the current passing through the system were monitored before, during and after the application of PEFs. A source-measuring unit (SMU, Keithley 2410) applied a constant DC voltage of 1 V and measured the resulting current before and after the PEF, while a digital oscilloscope (Tektronix MSO44), equipped with a high-voltage differential probe (Tektronix THDP0200) and an AC/DC current probe (Tektronix TCP0030A), measured the voltage applied on the electrodes and the current passing through the system during the application of the PEF. Instantaneous resistance is presented as voltage divided by current ($r(t)=u(t)/i(t)$). The temperature of the skin was monitored with a fiber optic temperature sensor (Neoptix Qualitrol), placed at the center, between the skin and the wet gauze, at the point with the highest current density and temperature increase.
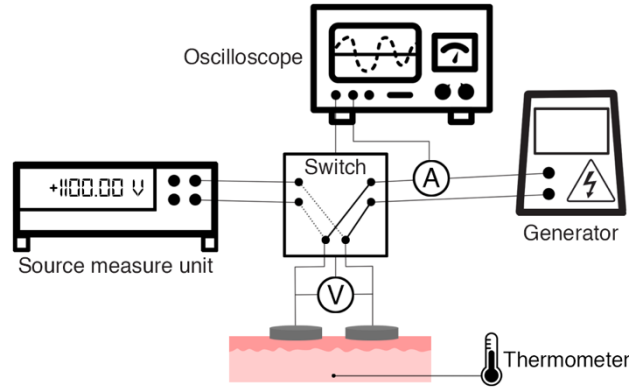
Fig. 2. Scheme of connections for *in situ* electrical measurements. Two hydrogels were placed on top of the skin model and connected to the pulse generator. An oscilloscope measured the voltage and current during the pulsed electric fields (PEF) application. Before, and after the PEF, the system was connected to a source-measuring unit (SMU) that measured the DC resistance. A manual switch allowed the transition between generator and SMU. The fiber optic temperature sensor was placed under the skin, at the center.

2.4 Numerical modeling

The current conservation continuity equation was solved with Finite Element Method (FEM) software (COMSOL Multiphysics, v. 6.1, AC/DC Module). The module solved the following set of equations in time domain:

$$\vec{E}(t) = -\vec{\nabla}V \tag{1}$$

$$\vec{J}(t) = \sigma\vec{E}(t) + \frac{\partial\vec{D}(t)}{\partial t} \tag{2}$$

With $\vec{E}(t)$ the electric field, V the voltage, $\vec{J}(t)$ the current density, σ the conductivity and $\vec{D}(t)$ the electric displacement. The geometry is described in **Fig. 5A** (stacked layers). The boundary conditions were the voltages set on each cylindrical electrical contact: the left cylinder was set at 0 V (ground) and the right cylinder was set at 50 to 400 V. For the purposes of the numerical simulation, the mouse skin was simulated as stacked layers, with homogeneous and isotropic conductivity. The conductivity of the skin layer with the highest resistance, the stratum corneum, can be increased up to three orders of magnitude during electroporation conditions [30]. We used the electrical measurements to adjust the nonlinear conductivity of the SC for different electric fields, while remaining within the range of the reported literature values. The temporal simulation with nonlinear conductivity for a very thin layer (SC) was challenging, especially to have a well-adapted mesh, therefore the grid was refined during the simulation to get a convergence of the solution. Earlier works have simulated this layer in larger dimensions, and compensated by increasing its conductivity [32], [53] or merged it with the rest of the epidermis [30]. The conductivity of the other skin layers also decreases through electroporation, but to a much lesser extent (factor of 2 to 4) [30]. This was not included in the simulation to save on computing power and because the changes in the global resistance of the system would be minor (<10%). Geometry and electrical properties of mouse skin were found in refs. [53], [54] (**Table 1**). In lack of data on the conductivity of specific mouse skin layers, the values from humans were used.
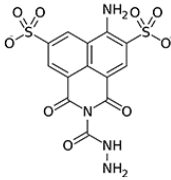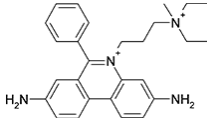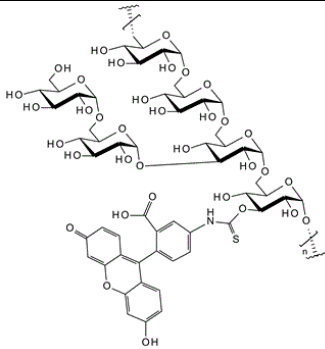
Table 1. Geometry and electrical properties of the different elements of the system.

	Thickness (m)	Conductivity (S/m)
Nanocomposite hydrogel	4×10^{-4}	0.15
Stratum corneum	9×10^{-6}	From 10^{-4} to 5×10^{-2}
Epidermis	1.8×10^{-5}	0.2
Dermis	1.8×10^{-4}	0.2
Hypodermis	10^{-4}	0.05
Muscle tissue	1.4×10^{-4}	0.5
Gauze with PBS	1×10^{-3}	1.5

2.5 Fluorescence macroscopy

After PEF application, the fluorophore-loaded hydrogels were left in contact with the mouse skin for 15 minutes, allowing for post-pulse delivery through diffusion. Once this time interval elapsed, the hydrogels were removed, and the mouse skins were thoroughly rinsed with PBS to wash away the fluorescent molecules that had not penetrated into the skin. The skin surface was visualized with an upright, wide-field fluorescence macroscope (MacroFluo with Light source EL6000, Leica Microsystems) equipped with a microscope camera (CoolSNAP HQ, Roper Scientific). The images, with magnifications of 0.57x up to 9.2x, were acquired through microscopy image analysis software (Metamorph, Molecular Devices) and treated through image processing software (ImageJ, National Institute of Health). A green filter cube (EX 480/40 nm, BS 505 nm, EM 527/30 nm; L5 filter, Leica Microsystems) was used for the FD4 and LY fluorophores, and a red filter cube (EX 560/40 nm, BS 585 nm, EM 630/75 nm; mCH/TR, Leica Microsystems) was used for PI. Exposure time was 1 s. Relative Fluorescence Intensity (RFI) is presented as a ratio between the mean fluorescence intensity of the treated area (full area under the hydrogel) divided by the mean fluorescence intensity of an untreated area of the mouse skin [23].

Table 2. Fluorescent molecules loaded into drug delivery hydrogels.

| Fluorophore	Molar mass (Da)	Charge	Notes	Chemical structure
Lucifer Yellow (LY)	457 (443 without 2 Li$^+$)	-2	Destabilization of extracellular matrix	
Propidium Iodide (PI)	668 (414 without 2 I$^-$)	+2	Cell permeabilization	
Fluorescein isothiocyanate–dextran (FD4)	4000 (avg)	Slightly -	Macromolecule delivery model	

2.6 Statistics

The fluorescence data was tested for normality, with the Shapiro-Wilk test and the distribution was found to be Gaussian or approximately Gaussian in all cases. The variance of the results was tested for equality with the Brown-Forsythe test and was found to be unequal for LY and PI and equal for FD4. Comparisons between relative fluorescence intensities of different treatment groups were made using one-way ANOVA, followed by the Dunnett's T3 post-hoc test, for the samples with unequal variance and the Dunnett's test for the sample with equal variance, and differences were considered significant for $p \leq 0.05$. The Dunnett's and Dunnett's T3 post-hoc tests are suitable for small groups and unequal sample sizes, which is the case for our fluorescence data. The Dunnett's test compares all groups to a control, while the Dunnett's T3 test compares all possible pairwise group differences and both tests are relatively conservative (limit false positives) [55].

3. Results and discussion

3.1 Electrical properties of the skin under PEF application

The application of a PEF, over a threshold value, permeabilizes the skin, creating aqueous pathways through the skin layers. These pathways allow the delivery of hydrophilic entities, such as hydrophilic drugs or fluorophores into the skin. At the same time, they also increase the conductivity of the skin by increasing the mobility of ions in the skin. Naturally present electrolytes (K^+, Na^+, Cl^- and others) give ionic conductive properties to tissues. However, in the SC, their mobility is dramatically restricted by the tightly packed lipid layers, resulting in a high resistivity ($\rho \approx 2000$ $\Omega \cdot m$). At the onset of electroporation, a measurable and rapid decrease in the instantaneous resistance of the system occurs.
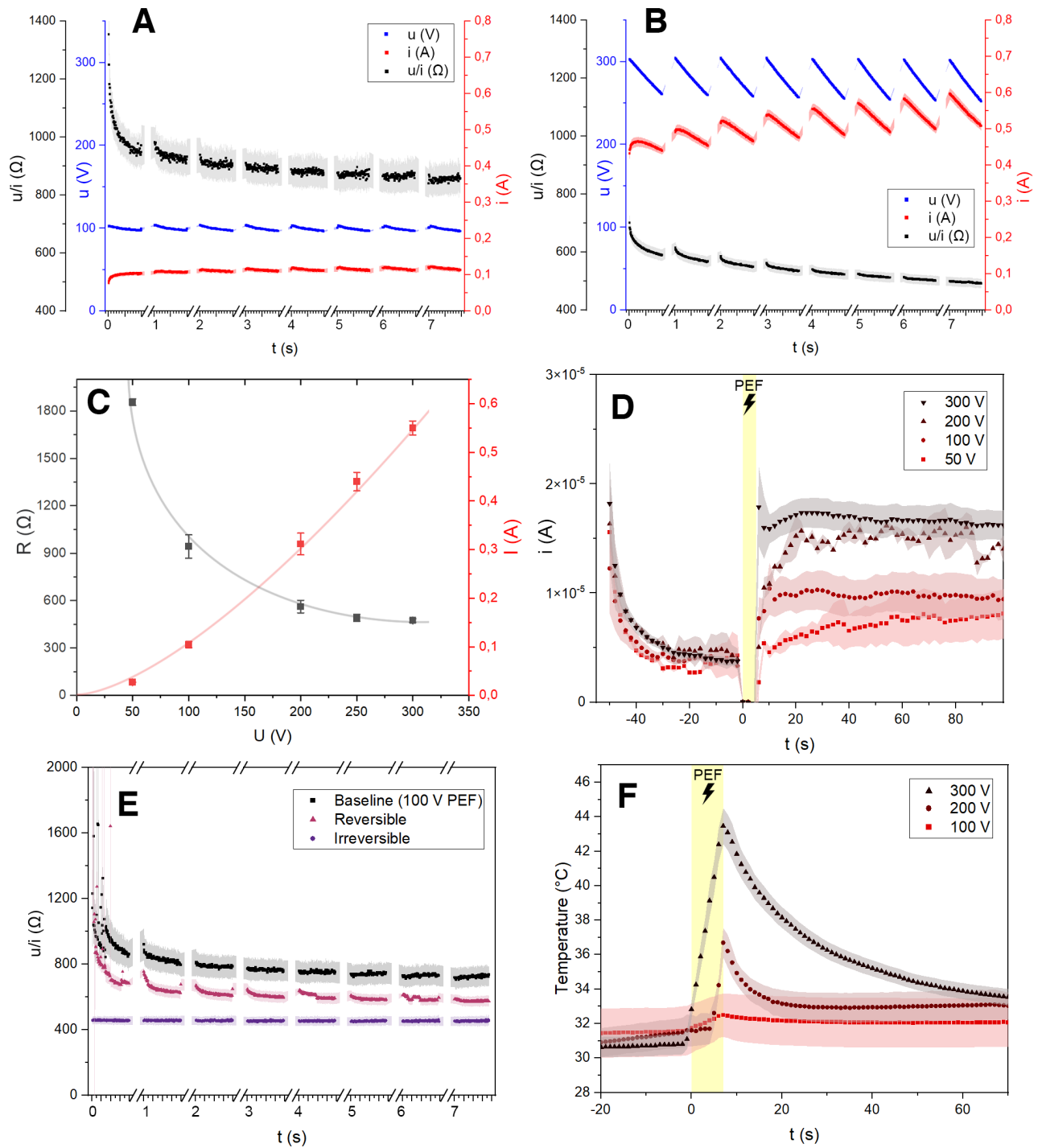
Fig. 3. Electrical properties and temperature increase of *ex vivo* mouse skin model, during PEF application. **(A)**, **(B)** Voltage, current and instantaneous resistance (u/i) of the systems during Pulsed Electric Fields (PEF) of 100 V (n=5) and 300 V (n=12). In both cases, the instantaneous resistance of the system decreases during pulse application, mostly for the first 5-7 ms. **(C)** I-V and R-V curves of the system, demonstrating non-linear behavior (n=2-18). **(D)** Electric current resulting from the application of 1V DC, before and after PEF (n=2-11). Yellow shaded area corresponds to PEF application. After a PEF of 50 V, the current does not change substantially. After PEF of 100 to 300 V, an increase in electric current was observed. **(E)** Instantaneous resistance of *ex vivo* system at 100 V, for a series of PEF applications (n=3-4). The instantaneous resistance of the skin after low-voltage PEF (up to 150 V) recovers near the baseline value. After, a series of high-voltage PEF (up to 400 V), the skin loses its dynamic character. **(F)** Temperature increase of the skin during PEF application (n=3-9). Yellow shaded area

10

corresponds to PEF application. The temperature increase is minimal for a PEF of 100 V, but increases considerably for 200 and 300 V. In all cases, shaded areas and error bars represent SEM.

We define the instantaneous resistance of the system as $r(t)=u(t)/i(t)$. The detailed electrical response obtained through the oscilloscope showed that the instantaneous resistance of the system decreased during the application of the pulses (**Fig. 3A**, **Fig. 3B** and Supplementary Info **Fig. S1** for the full data). A control experiment confirmed that the decrease in the instantaneous resistance of the system is attributed specifically to the skin, and not to the hydrogels or other components (wet gauze, metal electrical contacts, cables): the instantaneous resistance of our system without the skin remained constant during the application of PEFs (Supplementary Info, **Fig. S2**). This rapid decrease of resistance was attributed to the formation of LTRs, aqueous pathways that greatly increased ionic mobility and allowed the passage of hydrophilic molecules. The largest resistance decrease was observed during the first 5-7 ms after PEF application. We therefore infer that the expansion of the LTRs occurs within these first milliseconds. Further (lesser) decrease in instantaneous resistance may be attributed to conductivity changes within already formed and expanded LTRs, due to local temperature increase and lipid phase transition. According to molecular dynamics simulations, the creation of pores in the lipid bilayers of the SC takes place very rapidly, within few tens of nanoseconds (1-100 ns) [33]. It is possible that pores appear in the nano- to microsecond range, but their expansion continues up to the millisecond range.

Moreover, the average resistance of the system varied considerably for different applied voltages. The I/U graph (**Fig. 3C**) shows the average current and average resistance of the system, during the last of 8 pulses. It ranged from $1860 \pm 30\ \Omega$ for PEF of 50 V, down to $470 \pm 10\ \Omega$ during the application of 300 V PEF, indicating a highly non-linear electric behavior. There was a rapid decrease of average resistance between PEF of 50 to 100 V, then a more modest decrease till 200 V and minor further decrease for PEF up to 300 V. This multi-fold increase in conductivity was indicative of the extent of skin electroporation. We support the hypothesis that higher PEF voltages increased the density (the surface coverage) of LTRs in the skin, therefore increasing the overall conductivity.

Through the electrical measurements, we have also confirmed that the nanocomposite hydrogels establish effective electrical contact between the metal electrodes and the skin. This eliminated the necessity of using a conductive gel, as the resistance of the system remained unchanged regardless of the presence of a conductive gel (Supplementary Info, **Fig. S3**).

In parallel to the electrical response during PEF, we measured the current flowing through the system, under a 1 V DC square step chronoamperometry, before and after the PEF (**Fig. 3D**). Upon DC voltage application, a brief current peak was observed, decaying swiftly to a steady value. This peak was attributed to the formation and charging of an electrical double layer at the interfaces and the polarization of the system, while the steady state value corresponded to the conduction current [50], [56]. The current increased after the PEF treatment, indicating prolonged changes in the conductivity of the skin. The conduction current was equal to $4.0 \pm 0.1\ \mu A$ before PEF application. After PEF application, the current increased with the voltage applied: we measured $4.4 \pm 1.1\ \mu A$ (+10 %, not significant) for 50 V, $9.1 \pm 0.5\ \mu A$ (+130 %) for 100 V, $13.6 \pm 1.2\ \mu A$ (+240 %) for 200 V, and $16.3 \pm 0.3\ \mu A$ (+310 %) for 300 V. The current did not regress towards the baseline (current before PEF), even after up to 12 minutes following the application of PEF (Supplementary Info, **Fig. S4**).

Unexpectedly, the DC electrical properties of the skin did not recover, after PEF, even for the lower voltages tested (100 V; 50 V did not induce any significant changes). Similar studies have reported a rapid recovery (*ca.* 20 s for the essential part [57]). Some possible but unlikely explanations could be

the *ex vivo* system, not attached to the living organism; an influence of the 1 V DC applied, inhibiting electrical recovery, or a recovery in a later period.

3.2 Recovery of electrical properties of the skin after electroporation

Next, we studied the reversibility of the electrical response after the PEF application, by applying the PEF sequence to the same skin model multiple times. The first PEF application at 100 V, served as a baseline. For the reversibility experiment, we applied two sequences of low-to-moderate voltage PEF from 100 up to 150 V. For the irreversibility experiment, we applied five sequences of high-voltage PEF from 200 up to 400 V. The skin models were then placed in an incubator at 37 °C and left to recover for one hour. After the recovery, subsequent PEF at 100 V were applied and the electrical response was compared to the baseline (**Fig. 3E**). The instantaneous resistance of the baseline measurement started at 1200 ± 200 Ω, decreased to 860 ± 90 Ω at the end of the 1st pulse and further decreased to 730 ± 60 Ω at the last pulse. The reversible experiments revealed a similar behavior: the instantaneous resistance started at 1100 ± 100 Ω, decreased to 680 ± 20 Ω at the end of the 1st pulse and further decreased to 580 ± 30 Ω at the last pulse. The baseline and the reversibility experiments resulted in a typical instantaneous resistance behavior, with a major decrease over the first pulse and lesser subsequent decrease over the next pulses (compare with **Fig. 3A** and **Fig. 3B**). Moreover, the reversibility experiments indicated that the electrical properties of the skin were recovered, albeit not to 100 % of the baseline values (R/R_0=86%). The 14% loss in instantaneous resistance may include permanent formation of some conductive pathways, in the center of LTRs, due to local thermal damage or irreversible electrically-induced changes. On the contrary, after the irreversibility experiments, the skin exhibited a constant instantaneous resistance of 460 ± 20 Ω throughout the duration of the pulses. The instantaneous resistance of the skin not only did not recover to the baseline value (R/R_0=37%), but also totally lost its dynamic character, and was assimilated to a resistive material with a constant resistance, such as our system without the skin (consisting only of a wet gauze and hydrogels, compare **Fig. 3E** with **Fig. S2**). We infer that in this case, permanent conductive pathways were formed by a combination of electrical and thermal effects, in such density and size, that no new pathways could be formed for a PEF of 100 V, *i.e.* most of the current traversing the system passed through the pre-formed pathways.

3.3 Temperature and pH changes upon PEF application

The baseline temperature of the skin model was 31.2 ± 0.4 °C. During PEF application, the temperature of the explanted mouse skins increased rapidly throughout the duration of the pulses, before regressing towards baseline within the next seconds (**Fig. 3E**). There was no measurable increase for a PEF of 50 V. The max temperature reached 32.5 ± 1.3 °C for 100 V, 36.7 ± 0.9 °C for 200 V and 43.5 ± 1 °C for 300 V. In all cases, the maximum temperature was reached just after the last pulse of the PEF. The temperature decreased to less than 35 °C within 3 seconds, in the case of 200 V; and within 36 seconds, in the case of 300 V.

Electroporation is generally understood to be a non-thermal phenomenon at the lipid bilayer level [58]. Yet Joule heating, local temperature increase and heat transfer play an important role during the application of PEFs on biological tissue. The current passing through the skin produces heat. At the place with the highest current density (according to our numerical model) we measured a maximum temperature increase of +12.3 ± 1 °C for 300 V PEF, below the heat pain threshold on healthy human skin (50-55 °C [59]). For a fixed voltage, this increase can be minimized by decreasing the duration of the pulses and/or their frequency. *In vivo*, the temperature increase is expected to be lower, and the return to baseline faster, thanks to the mass of the organism that functions as a heat sink and blood circulation that contributes to thermoregulation. It must also be noted that the thermal properties of

mouse and human (thicker) skins should differ. Electroporation also induces heat shock protein activation in healthy tissue, but to a lesser extent than the exposure of tissue to a warm bath (40-45 °C) for few minutes [60].

The current density through the skin is not homogeneous. During PEF application, most of the SC retains its low conductivity, while LTRs have dramatically increased conductivities. As a result, the current density preferentially passes through these regions. The local temperature at the center of the transport regions may reach much higher values. According to Pliquett *et al.* [61] and Becker [62], the temperature locally rises to over 70 °C, the phase transition temperature of lipids, contributing to the thermal expansion of the LTR and the delivery of larger molecules. A local temperature increase as low as 45 °C can also contribute to the destabilization of the barrier function of the SC. At ~45 °C, the lipid packing transitions from orthorhombic to the less dense hexagonal packing [63]. In addition, Bulysheva *et al.* showed that moderately increased skin temperatures (43 °C) lead to more efficient cell permeabilisation, compared to a non-heated control (The temperature increase was independent from electric pulse application; they heated the skin through infrared laser heating) [36].

The exposure of an aqueous solution to a potential difference over 1.23 V causes pH changes due to water electrolysis. Higher voltages, such as the ones used in electroporation, accelerate the kinetics of electrolysis. We measured (qualitatively) the pH changes in the hydrogels and on the surface of the skin through the incorporation of phenol red in the hydrogels. The pH within the hydrogel buffer solution, and on the surface of the skin changed immediately after the PEF application, reaching values over 8.3 at the negative electrode and under 6.2 at the positive electrode (Supplementary Info, Fig. S5). In our configuration, the skin barrier function recovery would be impeded under the negative electrode, prolonging the duration of the LTRs. Neutral and alkaline pH hinder skin barrier recovery due to pH-related changes in the surface charge state of epidermal lipids, influencing their fusion rates [38] and/or impaired postsecretory lipid processing mediated by an acidic pH optimum of lipid-processing enzymes in the SC [37].

### 3.4 Numerical modeling of the skin upon PEF application

The numerical simulation allowed us to visualize the electric field distribution within the skin, during the PEF application. We used the *I/U* measurements (**Fig. 3C**) to adjust the relationship between the SC conductivity and the electric field, $\sigma_{SC}(E)$, until we got a satisfying agreement between the *ex vivo* results and the numerical model (**Fig. 4**), while remaining within the reported conductivity values for the SC under normal and electroporation conditions [32].

In all cases, the electric field was most intense in the areas directly under the hydrogels, reaching its highest values in the crescent-shaped areas where the electrodes face each other (**Fig. 5**). For PEFs at 50 and 100 V, the electric field in the viable skin layers (under the SC) did not reach sufficient levels for cell permeabilization. Starting at 200 V a very small part (6 %) of the treated area (area under the hydrogels) had values over the permeabilization threshold (400 V/cm [30]). At 300 V, most of the treated area (83 %) had values in the range of reversible permeabilization. At 400 V, all of the treated area had sufficiently high electric field, but the electric field exceeded the threshold for irreversible damage, in a small part of the treated area (7 %). The results are presented in **Fig. 5** and **Table 3** (full data can be found in SI **Fig. S6**)**.** As pointed out by Corovic *et al.*, the inclusion of nonlinear conductivity of the SC (*i.e.* the conductivity is dependent on the electric field, $\sigma(E)$) proves crucial for the electric field distribution [30]. With a constant conductivity, the electric field appeared to concentrate only on the SC, without reaching the viable skin layers (SI, **Fig. S6**).

The numerical model closely predicted the decrease in the average resistance of the system for increasing applied voltage, but we did not attempt to simulate the time-dependence of the

13

instantaneous resistance decrease during the pulses, which is connected to the expansion of aqueous pathways in the skin.

Another limit was the macroscopic nature of the numerical simulations. The electrical conductivity of the skin is not homogeneous and isotropic, as simulated. The increased conductivity is localized in LTRs. It is possible to take into account individual LTRs but the incomplete literature data on LTR conductivity, shape and density, as well as the imposed decreased model size due to computer power limitations, present their own shortcomings [64], [65]. Additionally, real skin contains imperfections, such as hair follicles and sweat ducts, which are areas of higher current density [66]. Moreover, the alignment of cells creates an anisotropic electrical conductivity. This is well established for muscle tissue, where the longitudinal conductivity can be up to 5 times higher than the transversal one [30], but the argument holds true for the cells of the SC too, and to a lesser extent, all of the skin. For these reasons, the exact values obtained from the simulations should be interpreted with caution.
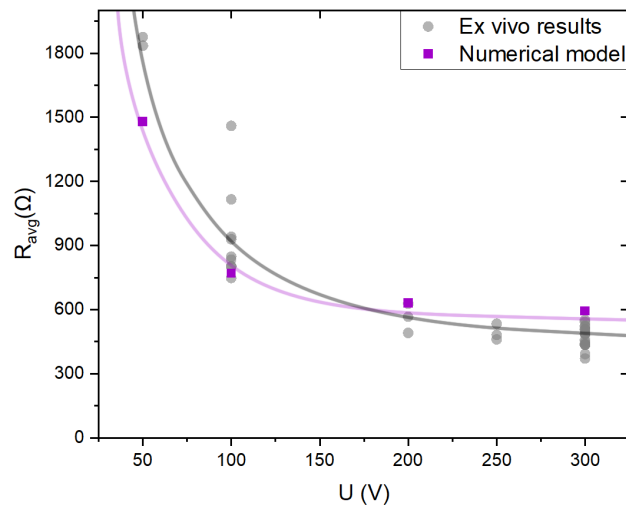
Fig. 4. Average resistance of the *ex vivo* system (grey circles) for applied PEF voltages from 50 to 300 V, compared with the results of the numerical model (purple squares).
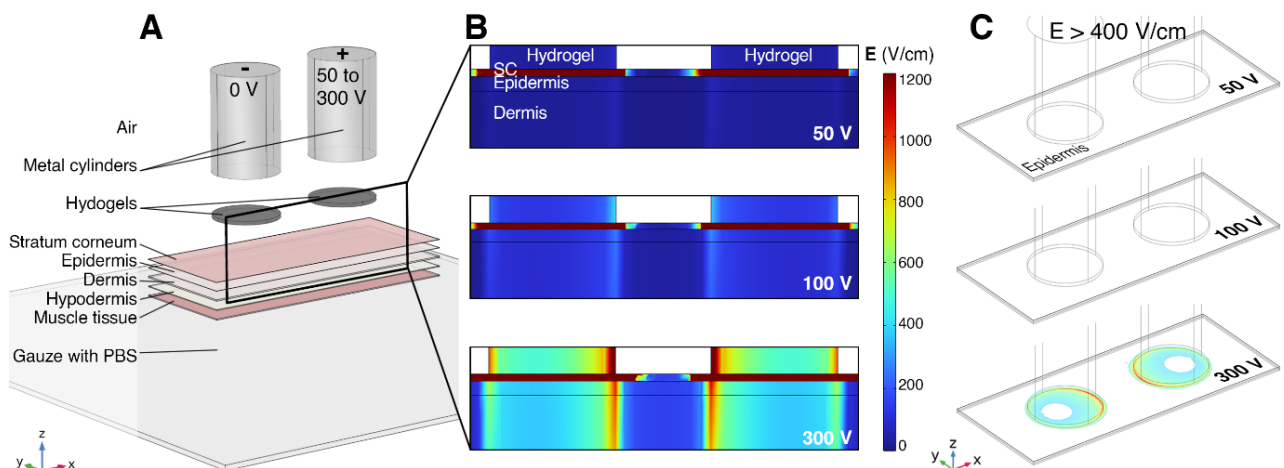
Fig. 5. Numerical simulation of mouse skin model during electrical stimulation. **(A)** The 3D drug delivery system (cascade layers preview, colorized). **(B)** XZ slices of electric field distribution for a PEF of 50, 100 and 300 V. **(C)** Viable skin (Epidermis, under the SC) area where the electric field is over the threshold value for cell permeabilization in tissue (~400 V/cm), for PEF of 50, 100 and 300 V. The color legend is common for B and C.

Table 3. Global resistance and electric field distribution in skin layers, for PEFs of 50 to 400 V. The threshold value for tissue electroporation is approx. 400 V/cm. For electric field values over 1200 V/cm, electroporation can be irreversible.

U (V)	R=U/I (Ω)	E (V/cm) @Viable skin	Rev perm. E>400 V/cm (% treated area)	Irrev. perm. E>1200 V/cm (% treated area)
50	1860	20-60	0	0
100	940	100-250	0	0
200	560	250-600	6	0
300	470	350-1000	83	0
400	450	500-1400	100	7

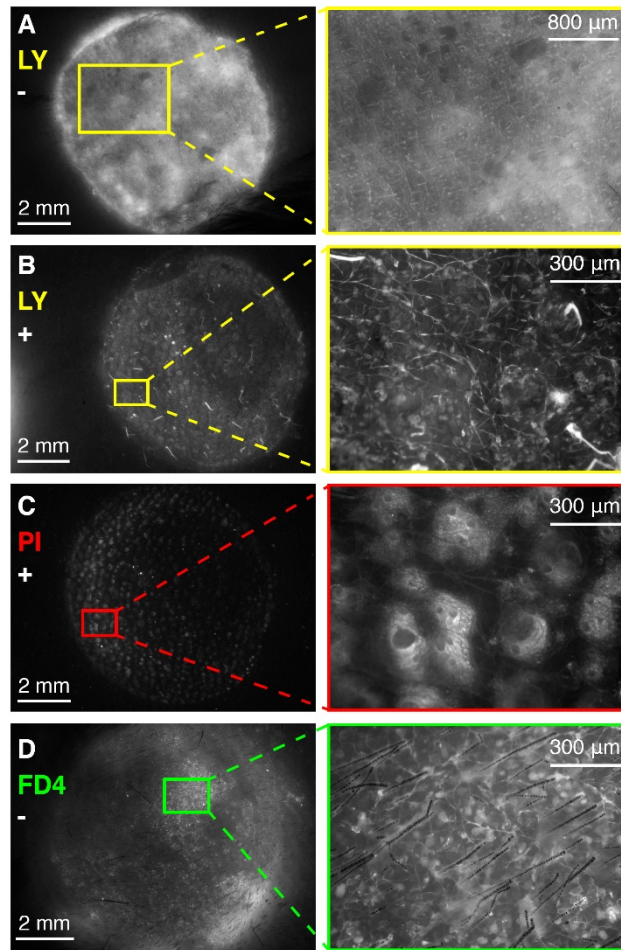### 3.5 Molecular delivery into skin after PEF application

Three fluorophores with different size, charge and properties were selected for the delivery tests assessed by fluorescence macroscopy (**Table 2**). For a range of PEF voltages studied, all three fluorophores demonstrated significantly higher fluorescence emission compared to the control. Lucifer Yellow (LY) is a small (442 Da), hydrophilic, negatively charged fluorophore. We used it as a marker of the integrity of the barrier function of the SC [67]. Under the positive electrode, there was no significant increase in the LY uptake for any of the PEF voltages tested. Under the negative electrode, LY exhibited a statistically significant (p=0.03; Dunnett's T3) increase in fluorescence (2.9 ± 0.4), compared to the control (1.4 ± 0.1), already at a PEF of 100 V. Further increase in the PEF voltage at 200 V resulted in an increased fluorescence emission (5.2 ± 0.3), while at 300 V, the fluorescence did not increase more (4.6 ± 0.3, **Fig. 6A**). Propidium Iodide (PI) is a small (668 Da), hydrophilic, positively-charged, membrane-impermeable, DNA-intercalating fluorophore, used here as evidence of cell membrane permeabilization. PI showed a statistically significant (p=0.0008; Dunnett's T3) increase in fluorescence only under the positive electrode, for a PEF of 300 V (1.54 ± 0.11, compared to 1.01 ± 0.02 for the control, **Fig. 6B**). Fluorescein isothiocyanate–dextran (FD4), is a large (4000 Da average molecular weight), hydrophilic fluorophore, with sparse negative charges (fluorescein is negatively charged and the substitution rate is *ca.* 0.01 mol FITC per mol of glucose). We used it as a model molecule for insulin, that has a comparable molecular weight (5700 Da). FD4 was only tested at 300 V, and showed a statistically significant (p=0.002; Dunnett's) increase in fluorescence, under the negative electrode (2.3 ± 0.3, compared to 0.96 ± 0.01 for the control, **Fig. 6C**). It should be noted that the luminescence intensity of fluorescein is reduced in acidic pH [68], and we measured an acidification of the solution in the positive electrode (SI, **Fig. S8**).
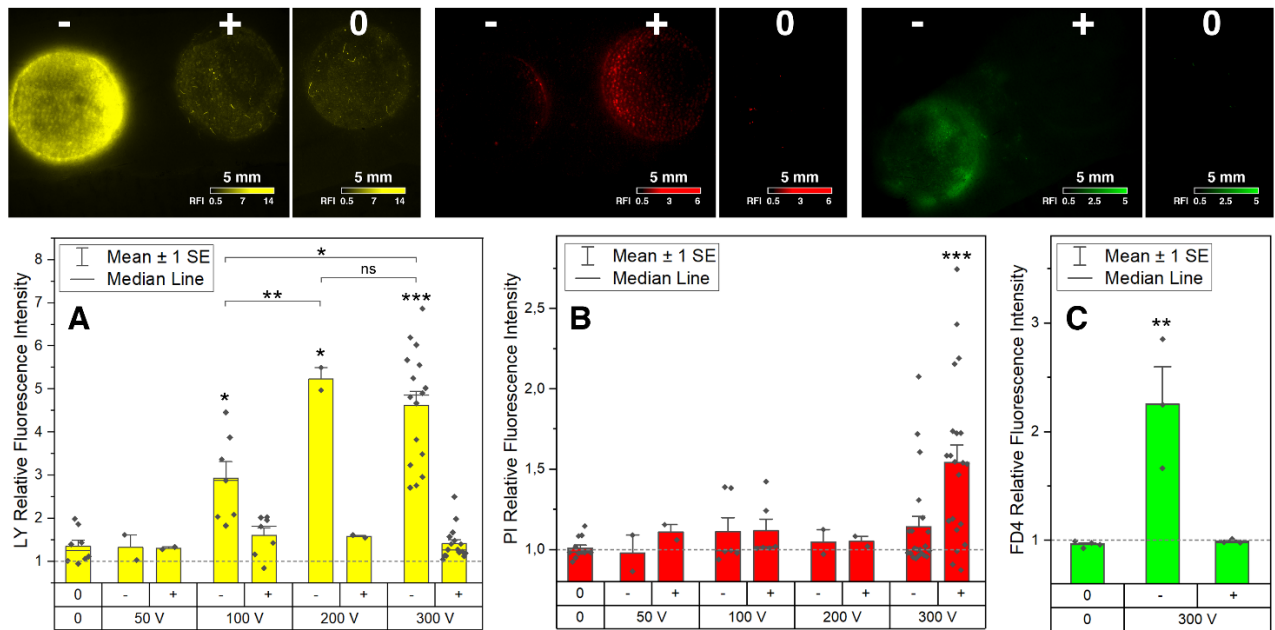
Fig. 6. Fluorescent molecule marking on skin model (top view) and relative fluorescence intensity quantification graphs. **(A)** Lucifer Yellow, a small (442 Da), negatively charged fluorophore penetrated the skin for PEF over 100 V (n=2-16). **(B)** Propidium Iodide, a small (668 Da), positively charged, DNA-intercalating fluorophore permeabilized nucleated cells for 300 V PEF (n=2-20). **(C)** Fluorescein isothiocyanate–dextran, a large (4000 Da), slightly negatively charged fluorophore was delivered through the skin with 300 V PEF (n=3-4). Error bars represent SEM. Statistical treatment: one-way ANOVA and Dunnett's T3 (A, B) or Dunnett's (C) post-hoc tests. Codes signification: * = p≤0.05; ** = p≤0.01; *** = p≤0.001; no symbol or ns = not significant difference (p>0.05). Means are compared to control (0), unless brackets indicate otherwise.

In all three cases, the charge of the fluorophore played a determining role in the delivery: negatively charged fluorophores marked the skin under the negative electrode and the positively charged PI mostly marked the skin under the positive electrode. This was true even for FD4, whose total electric charge was marginal. LY was the only fluorophore that exhibited some fluorescence in the control experiment. Indeed, the limit for passive diffusion through the SC, for hydrophilic molecules is approx. 500 Da. Molecules near this limit, like LY, have a very slow diffusion rate, but a small quantity can traverse the SC. However, the fluorescence of LY was greatly enhanced already with a PEF of 100 V. We hypothesized that the application of a PEF of 100 V, destabilized the extracellular lipids matrix between the corneocytes of the SC, allowing the fluorophore to pass through the paracellular pathway. An increase to 200 V nearly doubled the fluorescence intensity, while 300 V did not further increase it. The disorganization of the extracellular matrix peaked at 200 V, for our configuration. However, there was no cell membrane permeabilization for PEF lower than 300 V. PI, a marker of cell permeabilization, only exhibited enhanced fluorescence at 300 V. PI is a DNA intercalating agent, increasing its fluorescence by 20- to 30-fold when it binds to DNA [69]. The cells of the SC do not contain a nucleus, thus the PI fluorescence originated in cells in deeper layers of the epidermis or the dermis. Lastly, FD4, a macromolecule of 4 kDA, exhibited significantly increased fluorescence, demonstrating the potential of skin electroporation for the delivery of therapeutic molecules of large size, such as insulin [23].

Fig. 7. Molecular delivery into skin model after PEF at 300 V. Images showing the patterns of fluorescence with **(A)** Lucifer Yellow (LY) under negative electrode with optical zoom of 1.25x (left) and 3.2x (right); **(B)** LY under positive electrode with optical zoom of 1.25x (left) and 9.2x (right); **(C)** Propidium Iodide (PI) under positive electrode with optical zoom of 1.25x (left) and 9.2x (right); **(D)** Fluorescein isothiocyanate–dextran under negative electrode with optical zoom of 1.25x (left) and 9.2x (right). LY fluorescence mostly originates from the paracellular space of the stratum corneum (B), while Propidium Iodide is located in the intracellular space of nucleated cells, in the viable skin (C). Brightness and contrast are customized for each capture.

Visible light penetrates into the skin, at a depth of few hundred μm, typically 100 μm to 1 mm, depending on the wavelength [70]. Therefore, fluorescence emission captured by the camera does not only originate from the SC, but also from deeper layers, at least down to parts of the dermis. Under the negative electrode, the fluorescence of LY appeared mostly concentrated at the regions between cells. Additionally, a diffuse, out-of-focus fluorescence was observed, originating from LY deeper into the skin (**Fig. 7A**). Under the positive electrode, where LY did not benefit from the electrophoretic force, it was clearly seen concentrated on the paracellular regions, with much less diffuse light from deeper layers (**Fig. 7B**). PI was observed within skin cells (**Fig. 7C**). The cells of the SC are anucleated, thus PI fluorescence originated from cells deeper in the epidermis and/or dermis. Similar to LY, FD4 appeared to fluoresce from the paracellular regions, with some diffuse light from deeper layers (**Fig. 6D**). In most cases, the fluorescence intensity was higher in the crescent-shaped areas where electrodes face each other. This can be explained by the electric field strength calculated through the simulations, which was higher in these areas (**Fig. 5C**).

3.6 Mechanisms of skin electroporation

We evaluated skin electroporation, for applied PEFs of 50 to 300 V, on four different levels: (1) electrical measurements during the pulses, (2) DC current before and after the pulses, (3) fluorescent microscopy of LY, a fluorophore indicating destabilization of skin's barrier properties, and (4) fluorescent microscopy of PI for cell membrane permeabilization. Combining our findings, we distinguish three voltage domains with different effects on the skin.

### Domain 1: low-voltage PEFs (<100 V) - Conductive pathway formation

In the initial domain, where PEFs were below 100 V, an increase in ionic mobility within the skin was observed. This was evidenced by a reduction in instantaneous resistance during PEFs and a decline in average resistance with increasing voltage. Remarkably, these effects were noticeable even at PEFs as low as 50 V. However, no molecule transfer through the skin occurred at voltages less than 100 V. We hypothesize that the conductive pathways formed within the skin increased the mobility of electrolytes but were too small in radius or limited in surface coverage to impact the skin's barrier properties (**Fig. 8B**). Additionally, the DC current measured before and after applying 50 V PEFs showed minimal alterations (not significant), suggesting that any changes in electrical properties were short-lived. It was challenging to establish a precise minimum PEF voltage threshold for pathway formation, based solely on electrical properties, as instantaneous resistance decreased even at the lowest voltages applied. According to Chizmadzhev *et al.*, at low voltages (up to 30 V, equivalent to roughly 100 V in our configuration, see SI **Fig. S7** for the equivalence calculation), electroporation of epithelial cells in appendageal ducts might contribute to the observed reduction in skin resistance. The appendageal ducts (hair follicles and sweat ducts) are areas of higher current density and are lined by only two layers of epithelial cells [66].

Domain 2: moderate-voltage PEFs (100-200 V) – Disruption of extracellular lipid matrix and molecule transport

Moving to the second domain, encompassing PEFs ranging from 100 to 200 V, we observed the transport of small hydrophilic molecules through the SC and enduring changes in the skin's passive electrical properties. At this stage, the applied PEF disrupted the organization of extracellular lipids in the SC, resulting in the formation of LTRs. Hydrophilic molecules with limited passive diffusion through the SC, such as LY, traversed the SC via the disorganized lipid bilayers in the paracellular region (**Fig. 8C**). Moreover, we noted an increase in the skin's DC current following PEF application, indicating the sustained creation of conductive pathways. Still, no permeabilization of cell membranes occurred within this domain.

Domain 3: high-voltage PEFs (300 V) - Cell membrane permeabilization

In the third domain, corresponding to PEFs of 300 V, we observed the permeabilization of cell membranes. At this point, the electric field at the viable skin layers reached values exceeding 400 V/cm. This resulted in a transmembrane potential within nucleated cells in the epidermis and/or dermis surpassing the threshold of 250 mV, leading to membrane permeabilization. This allowed the introduction of Propidium Iodide (PI) into the intracellular space, followed by its subsequent intercalation with DNA (**Fig. 8D**). Our numerical simulations, despite their simplifications, accurately predicted cell membrane permeabilization for 300 V PEFs. In previous work, we assessed the uptake of LY following PEF exposure and established that PEFs of 300 V, within our configuration, were largely reversible [23].
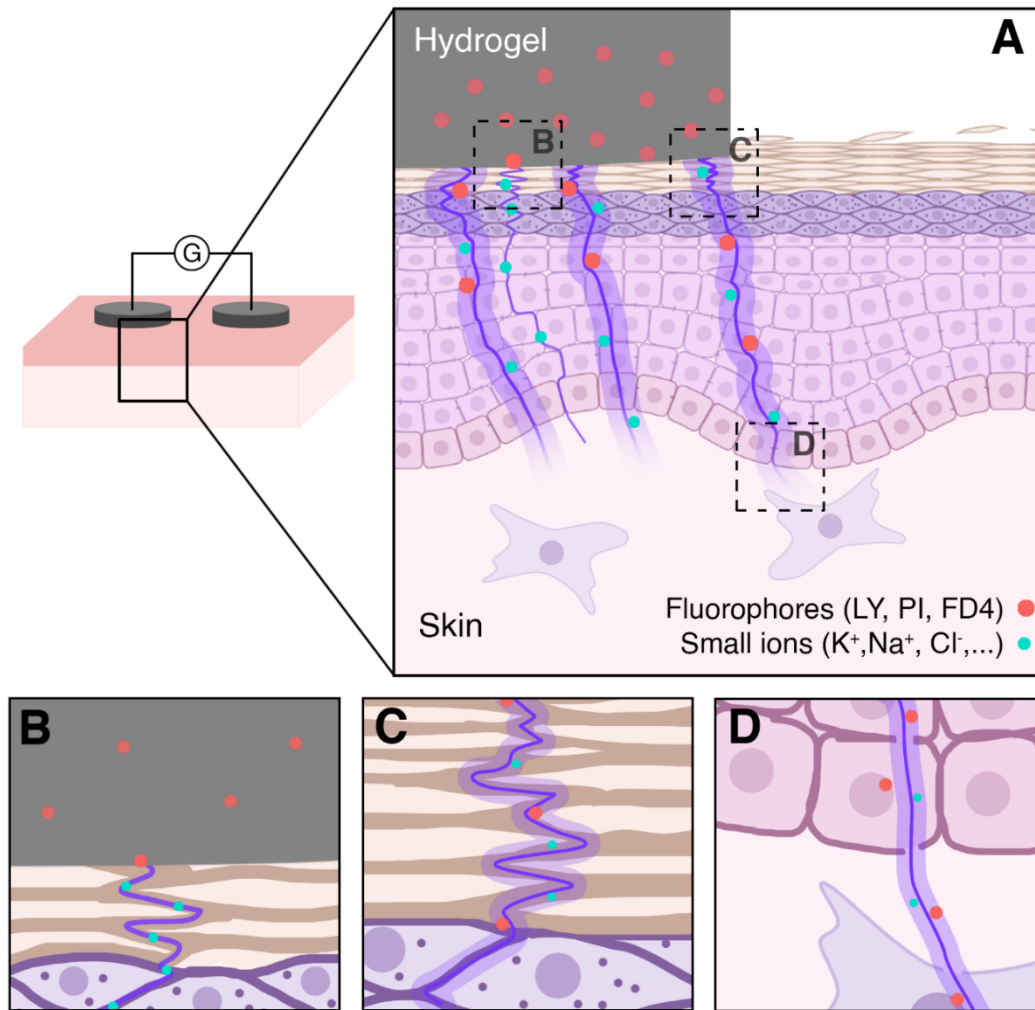
Fig. 8. Local transport regions (LTRs) and cell membrane permeabilization in skin. **(A)** Scheme of skin electroporation with electrode-reservoir hydrogel. **(B)** At PEF voltages lower than 100 V, conductive pathways were formed, increasing ionic mobility. **(C)** Starting at 100 V PEF, the creation of LTRs in the extracellular lipids of the stratum corneum, allowed the diffusion of fluorophores through the skin. **(D)** At 300 V PEF, the cell membranes of nucleated cells of the epidermis and/or dermis were permeabilized and fluorophores entered the cytoplasm.

4. Conclusion

We have proposed a configuration for non-invasive drug delivery through skin electroporation, consisting of two conductive hydrogels, placed side-to-side, that contain the model medication and serve as electrodes for the application of electrical pulses on the skin. We applied a multi-scale approach to evaluate skin electroporation and drug delivery: *in situ* measurements of electrical properties and temperature before, during and after the application of PEFs, FEM simulation of our system and fluorescence microscopy to evaluate the delivery of model molecules (A schematic table with the summarized results is provided in SI, **Fig. S8**). The experimental setup proposed here can serve as a model for future investigations of skin electroporation.

Regarding the I-V measurements, there were two major observations: (1) the average resistance of the system decreased for increasing PEF voltages, and (2) the instantaneous resistance of the system decreased during the application of the electric pulses. We attributed the first observation to the formation of a larger number of LTRs with increasing applied voltage, and the second observation to

the expansion of the LTRs during the electric field application. The current-voltage graph of the system demonstrated the non-linear character of the skin's electrical conductivity. There was a substantial local temperature increase for PEFs over 200 V, but the skin temperature remained under the limits of human heat pain threshold, for PEFs up to 300 V. We used electrical measurements to evaluate the reversibility of PEF application on our configuration: low PEF voltages up to 150 V resulted in near-full recovery of the skin's instantaneous resistance, while multiple sequences of high PEF voltages up to 400 V, irreversibly damaged the skin and its dynamic electrical behavior.

The numerical model was adjusted with *ex vivo* results and accurately predicted the evolution of the average resistance of the system for increasing applied voltage. According to the model, the electric field reached levels of reversible cell permeabilization in the viable skin layers, for most of the treated area, at 300 V PEF. At 400 V, the field strength passed the threshold for irreversible electroporation (eventually leading to cell death), in parts of the treated area.

Even though the formation of LTRs within the SC was demonstrated for PEFs starting at 100 V, no permeabilization of nucleated cells was observed for PEFs lower than 300 V. These results showed the existence of two distinct (reversible) electroporation domains, one consisting in the formation of LTRs in the extracellular lipids of the SC and the accompanying increase in skin's conductivity, and a second one, consisting in the permeabilization of the plasma membranes of nucleate cells (*i.e.* cells in layers deeper than the SC). Both of these domains are relevant in the context of drug delivery through the skin. Some drugs such as lidocaine and corticosteroids can be administered locally, to the epidermis, for local anesthesia and to treat skin inflammation. Nucleic acid vaccinations have to enter the interior of cells in order to express the encoded antigen and elicit an immune response. Similarly, antitumor antibiotic medicine like bleomycin, have to permeabilize the cell membrane to have an effect. Fentanyl and insulin have to reach systemic circulation, through the vasculature of the dermis, to treat pain and regulate glucose metabolism. The exact parameters chosen for skin electroporation depend on the delivery target and the drug's physicochemical properties (size, charge, hydrophilicity).

Abbreviations

PEF	Pulsed Electric Field
SC	Stratum Corneum
LTR	Local Transport Region
CNT	Carbon Nanotube
LY	Lucifer Yellow
PI	Propidium Iodide
FD4	Fluorescein isothiocyanate–dextran (MW: 4kDA)

Author Contributions

Conceptualization: GK, MG, LL, ZVN, EF; Methodology: GK, JS, SD, LL; Formal analysis: GK; Investigation: GK, LL; Writing - original draft: GK; Writing - review and editing: SD, MG, LL, ZVN, EF; Visualization: GK; Supervision: ZVN, EF; Funding acquisition: MG, ZVN, EF

Conflicts of Interest

There are no conflicts to declare.

Acknowledgements

References

[1] G. W. Cleary, « Transdermal Delivery Systems: A Medical Rationale », in *Topical Drug Bioavailability, Bioequivalence, and Penetration*, V. P. Shah et H. I. Maibach, Éd., Boston, MA: Springer US, 1993, p. 17-68. doi: 10.1007/978-1-4899-1262-6_2.

[2] A.-R. Denet, R. Vanbever, et V. Préat, « Skin electroporation for transdermal and topical delivery », *Adv. Drug Deliv. Rev.*, vol. 56, nᵒ 5, p. 659-674, mars 2004, doi: 10.1016/j.addr.2003.10.027.

[3] S. Wiedersberg et R. H. Guy, « Transdermal drug delivery: 30+ years of war and still fighting! », *J. Controlled Release*, vol. 190, p. 150-156, sept. 2014, doi: 10.1016/j.jconrel.2014.05.022.

[4] R. Vanbever et V. Préat, « In vivo efficacy and safety of skin electroporation », *Adv. Drug Deliv. Rev.*, vol. 35, nᵒ 1, p. 77-88, janv. 1999, doi: 10.1016/s0169-409x(98)00064-7.

[5] M. R. Prausnitz, « A practical assessment of transdermal drug delivery by skin electroporation », *Adv. Drug Deliv. Rev.*, vol. 35, nᵒ 1, p. 61-76, janv. 1999, doi: 10.1016/s0169-409x(98)00063-5.

[6] J. Dermol-Černe, E. Pirc, et D. Miklavčič, « Mechanistic view of skin electroporation – models and dosimetry for successful applications: an expert review », *Expert Opin. Drug Deliv.*, vol. 17, nᵒ 5, p. 689-704, mai 2020, doi: 10.1080/17425247.2020.1745772.

[7] J. A. McGrath, R. a. J. Eady, et F. M. Pope, « Anatomy and Organization of Human Skin », in *Rook's Textbook of Dermatology*, John Wiley & Sons, Ltd, 2004, p. 45-128. doi: 10.1002/9780470750520.ch3.

[8] E. Candi, R. Schmidt, et G. Melino, « The cornified envelope: a model of cell death in the skin », *Nat. Rev. Mol. Cell Biol.*, vol. 6, nᵒ 4, Art. nᵒ 4, avr. 2005, doi: 10.1038/nrm1619.

[9] M. R. Prausnitz, V. G. Bose, R. Langer, et J. C. Weaver, « Electroporation of mammalian skin: a mechanism to enhance transdermal drug delivery. », *Proc. Natl. Acad. Sci.*, vol. 90, nᵒ 22, p. 10504-10508, nov. 1993, doi: 10.1073/pnas.90.22.10504.

[10] Y. Gilaberte, L. Prieto-Torres, I. Pastushenko, et Á. Juarranz, « Chapter 1 - Anatomy and Function of the Skin », in *Nanoscience in Dermatology*, M. R. Hamblin, P. Avci, et T. W. Prow, Éd., Boston: Academic Press, 2016, p. 1-14. doi: 10.1016/B978-0-12-802926-8.00001-X.

[11] E. Neumann et K. Rosenheck, « Permeability changes induced by electric impulses in vesicular membranes », *J. Membr. Biol.*, vol. 10, nᵒ 1, p. 279-290, déc. 1972, doi: 10.1007/BF01867861.

[12] T. Kotnik, L. Rems, M. Tarek, et D. Miklavčič, « Membrane Electroporation and Electropermeabilization: Mechanisms and Models », *Annu. Rev. Biophys.*, vol. 48, nᵒ 1, p. 63-91, 2019, doi: 10.1146/annurev-biophys-052118-115451.

[13] S. Chabot, C. Rosazza, M. Golzio, A. Zumbusch, J. Teissié, et M.-P. Rols, « Nucleic acids electro-transfer: from bench to bedside », *Curr. Drug Metab.*, vol. 14, nᵒ 3, p. 300-308, mars 2013, doi: 10.2174/1389200211314030005.

[14] I. P. Sugar, W. Förster, et E. Neumann, « Model of cell electrofusion: Membrane electroporation, pore coalescence and percolation », *Biophys. Chem.*, vol. 26, nᵒ 2, p. 321-335, mai 1987, doi: 10.1016/0301-4622(87)80033-9.

[15] L. M. Mir *et al.*, « Effective treatment of cutaneous and subcutaneous malignant tumours by electrochemotherapy », *Br. J. Cancer*, vol. 77, nᵒ 12, Art. nᵒ 12, juin 1998, doi: 10.1038/bjc.1998.388.

[16] S. Pedron-Mazoyer, J. Plouët, L. Hellaudais, J. Teissie, et M. Golzio, « New anti angiogenesis developments through electro-immunization: optimization by in vivo optical imaging of

intradermal electro gene transfer », *Biochim. Biophys. Acta*, vol. 1770, n° 1, p. 137-142, janv. 2007, doi: 10.1016/j.bbagen.2006.09.014.

[17] L. Pasquet *et al.*, « Safe and efficient novel approach for non-invasive gene electrotransfer to skin », *Sci. Rep.*, vol. 8, n° 1, Art. n° 1, nov. 2018, doi: 10.1038/s41598-018-34968-6.

[18] B. M. Medi, B. Layek, et J. Singh, « Electroporation for Dermal and Transdermal Drug Delivery », in *Percutaneous Penetration Enhancers Physical Methods in Penetration Enhancement*, N. Dragicevic et H. I. Maibach, Éd., Berlin, Heidelberg: Springer, 2017, p. 105-122. doi: 10.1007/978-3-662-53273-7_7.

[19] R. Vanbever, N. Lecouturier, et V. Préat, « Transdermal Delivery of Metoprolol by Electroporation », *Pharm. Res.*, vol. 11, n° 11, p. 1657-1662, nov. 1994, doi: 10.1023/A:1018930425591.

[20] A. Jadoul, N. Lecouturier, J. Mesens, W. Caers, et V. Préat, « Transdermal alniditan delivery by skin electroporation », *J. Controlled Release*, vol. 54, n° 3, p. 265-272, août 1998, doi: 10.1016/S0168-3659(97)00195-8.

[21] V. Regnier, N. De Morre, A. Jadoul, et V. Préat, « Mechanisms of a phosphorothioate oligonucleotide delivery by skin electroporation », *Int. J. Pharm.*, vol. 184, n° 2, p. 147-156, juill. 1999, doi: 10.1016/S0378-5173(98)00085-4.

[22] T.-W. Wong, T.-Y. Chen, C.-C. Huang, J.-C. Tsai, et S. W. Hui, « Painless Skin Electroporation as a Novel Way for Insulin Delivery », *Diabetes Technol. Ther.*, vol. 13, n° 9, p. 929-935, sept. 2011, doi: 10.1089/dia.2011.0077.

[23] J. Simon, B. Jouanmiqueou, M.-P. Rols, E. Flahaut, et M. Golzio, « Transdermal Delivery of Macromolecules Using Two-in-One Nanocomposite Device for Skin Electroporation », *Pharmaceutics*, vol. 13, n° 11, Art. n° 11, nov. 2021, doi: 10.3390/pharmaceutics13111805.

[24] N. Kis, A. Kovács, M. Budai-Szűcs, G. Erős, E. Csányi, et S. Berkó, « The effect of non-invasive dermal electroporation on skin barrier function and skin permeation in combination with different dermal formulations », *J. Drug Deliv. Sci. Technol.*, vol. 69, p. 103161, mars 2022, doi: 10.1016/j.jddst.2022.103161.

[25] M. Madi, M.-P. Rols, et L. Gibot, « Efficient In Vitro Electropermeabilization of Reconstructed Human Dermal Tissue », *J. Membr. Biol.*, vol. 248, n° 5, p. 903-908, oct. 2015, doi: 10.1007/s00232-015-9791-z.

[26] M. S. Wallace, B. Ridgeway, E. Jun, G. Schulteis, D. Rabussay, et L. Zhang, « Topical Delivery of Lidocaine in Healthy Volunteers by Electroporation, Electroincorporation, or Iontophoresis: An Evaluation of Skin Anesthesia », *Reg. Anesth. Pain Med.*, vol. 26, n° 3, p. 229-238, mai 2001, doi: 10.1053/rapm.2001.22633.

[27] U. Pliquett et J. C. Weaver, « Feasibility of an electrode-reservoir device for transdermal drug delivery by noninvasive skin electroporation », *IEEE Trans. Biomed. Eng.*, vol. 54, n° 3, p. 536-538, mars 2007, doi: 10.1109/TBME.2006.886828.

[28] J. Teissié et M. P. Rols, « An experimental evaluation of the critical potential difference inducing cell membrane electropermeabilization. », *Biophys. J.*, vol. 65, n° 1, p. 409-413, juill. 1993.

[29] M. Tarek, « Membrane Electroporation: A Molecular Dynamics Simulation », *Biophys. J.*, vol. 88, n° 6, p. 4045-4053, juin 2005, doi: 10.1529/biophysj.104.050617.

[30] S. Corovic, I. Lackovic, P. Sustaric, T. Sustar, T. Rodic, et D. Miklavcic, « Modeling of electric field distribution in tissues during electroporation », *Biomed. Eng. OnLine*, vol. 12, n° 1, p. 16, févr. 2013, doi: 10.1186/1475-925X-12-16.

[31] U. F. Pliquett, T. E. Zewert, T. Chen, R. Langer, et J. C. Weaver, « Imaging of fluorescent molecule and small ion transport through human stratum corneum during high voltage pulsing: localized transport regions are involved », *Biophys. Chem.*, vol. 58, n° 1, p. 185-204, janv. 1996, doi: 10.1016/0301-4622(95)00098-4.

[32] N. Pavšelj, V. Préat, et D. Miklavčič, « A Numerical Model of Skin Electropermeabilization Based on In Vivo Experiments », *Ann. Biomed. Eng.*, vol. 35, n° 12, p. 2138-2144, déc. 2007, doi: 10.1007/s10439-007-9378-7.

[33] R. Gupta et B. Rai, « Electroporation of Skin Stratum Corneum Lipid Bilayer and Molecular Mechanism of Drug Transport: A Molecular Dynamics Study », *Langmuir*, vol. 34, n° 20, p. 5860-5870, mai 2018, doi: 10.1021/acs.langmuir.8b00423.

[34] B. Zorec, V. Préat, D. Miklavčič, et N. Pavselj, « Active enhancement methods for intra- and transdermal drug delivery: a review. », *ZdravVestn*, 2013, doi: 10.6016/1889.

[35] S. Narasimha Murthy, A. Sen, Y.-L. Zhao, et S. W. Hui, « Temperature Influences the Postelectroporation Permeability State of the Skin », *J. Pharm. Sci.*, vol. 93, n° 4, p. 908-915, avr. 2004, doi: 10.1002/jps.20016.

[36] A. Bulysheva *et al.*, « Coalesced thermal and electrotransfer mediated delivery of plasmid DNA to the skin », *Bioelectrochemistry Amst. Neth.*, vol. 125, p. 127-133, févr. 2019, doi: 10.1016/j.bioelechem.2018.10.004.

[37] T. Mauro *et al.*, « Barrier recovery is impeded at neutral pH, independent of ionic effects: implications for extracellular lipid processing », *Arch. Dermatol. Res.*, vol. 290, n° 4, p. 215-222, avr. 1998, doi: 10.1007/s004030050293.

[38] S. N. Murthy, A. Sen, Y.-L. Zhao, et S. W. Hui, « pH influences the postpulse permeability state of skin after electroporation », *J. Controlled Release*, vol. 93, n° 1, p. 49-57, nov. 2003, doi: 10.1016/j.jconrel.2003.08.002.

[39] S. N. Murthy, A. Sen, et S. W. Hui, « Surfactant-enhanced transdermal delivery by electroporation », *J. Controlled Release*, vol. 98, n° 2, p. 307-315, août 2004, doi: 10.1016/j.jconrel.2004.05.006.

[40] A. Sen, Y. Zhao, L. Zhang, et S. W. Hui, « Enhanced transdermal transport by electroporation using anionic lipids », *J. Controlled Release*, vol. 82, n° 2, p. 399-405, août 2002, doi: 10.1016/S0168-3659(02)00164-5.

[41] A. Sen, M. E. Daly, et S. W. Hui, « Transdermal insulin delivery using lipid enhanced electroporation », *Biochim. Biophys. Acta BBA - Biomembr.*, vol. 1564, n° 1, p. 5-8, août 2002, doi: 10.1016/S0005-2736(02)00453-4.

[42] T. E. Zewert, U. F. Pliquett, R. Vanbever, R. Langer, et J. C. Weaver, « Creation of transdermal pathways for macromolecule transport by skin electroporation and a low toxicity, pathway-enlarging molecule », *Bioelectrochem. Bioenerg.*, vol. 49, n° 1, p. 11-20, oct. 1999, doi: 10.1016/S0302-4598(99)00056-2.

[43] J. C. Weaver, R. Vanbever, T. E. Vaughan, et M. R. Prausnitz, « Heparin Alters Transdermal Transport Associated with Electroporation », *Biochem. Biophys. Res. Commun.*, vol. 234, n° 3, p. 637-640, mai 1997, doi: 10.1006/bbrc.1997.6701.

[44] R. Vanbever, M. R. Prausnitz, et V. Préat, « Macromolecules as novel transdermal transport enhancers for skin electroporation », *Pharm. Res.*, vol. 14, n° 5, p. 638-644, mai 1997, doi: 10.1023/a:1012161313701.

[45] G. A. Hofmann, W. V. Rustrum, et K. S. Suder, « Electro-incorporation of microcarriers as a method for the transdermal delivery of large molecules », *Bioelectrochem. Bioenerg.*, vol. 38, n° 1, p. 209-222, août 1995, doi: 10.1016/0302-4598(95)01827-2.

[46] J.-F. Guillet, E. Flahaut, et M. Golzio, « A Hydrogel/Carbon-Nanotube Needle-Free Device for Electrostimulated Skin Drug Delivery », *ChemPhysChem*, vol. 18, n° 19, p. 2715-2723, 2017, doi: https://doi.org/10.1002/cphc.201700517.

[47] S. Mazères *et al.*, « Non invasive contact electrodes for in vivo localized cutaneous electropulsation and associated drug and nucleic acid delivery », *J. Control. Release Off. J. Control. Release Soc.*, vol. 134, n° 2, p. 125-131, mars 2009, doi: 10.1016/j.jconrel.2008.11.003.

[48] S. Guo, A. Donate, G. Basu, C. Lundberg, L. Heller, et R. Heller, « Electro-gene transfer to skin using a noninvasive multielectrode array », *J. Control. Release Off. J. Control. Release Soc.*, vol. 151, n° 3, p. 256-262, mai 2011, doi: 10.1016/j.jconrel.2011.01.014.

[49] L. Zhang, L. Li, Z. An, R. M. Hoffman, et G. A. Hofmann, « In vivo transdermal delivery of large molecules by pressure-mediated electroincorporation and electroporation: a novel method for drug and gene delivery », *Bioelectrochem. Bioenerg.*, vol. 42, n° 2, p. 283-292, mai 1997, doi: 10.1016/S0302-4598(96)05128-8.

[50] G. Kougkolos, M. Golzio, L. Laudebat, Z. Valdez-Nava, et E. Flahaut, « Hydrogels with electrically conductive nanomaterials for biomedical applications », *J. Mater. Chem. B*, vol. 11, n° 10, p. 2036‑2062, mars 2023, doi: 10.1039/D2TB02019J.

[51] J.-F. Guillet, Z. Valdez-Nava, M. Golzio, et E. Flahaut, « Electrical properties of double-wall carbon nanotubes nanocomposite hydrogels », *Carbon*, vol. 146, p. 542‑548, mai 2019, doi: 10.1016/j.carbon.2019.01.090.

[52] C. M. Lee, S.-P. Jin, E. J. Doh, D. H. Lee, et J. H. Chung, « Regional Variation of Human Skin Surface Temperature », *Ann. Dermatol.*, vol. 31, n° 3, p. 349‑352, juin 2019, doi: 10.5021/ad.2019.31.3.349.

[53] N. Pavselj et D. Miklavcic, « Numerical Models of Skin Electropermeabilization Taking Into Account Conductivity Changes and the Presence of Local Transport Regions », *Plasma Sci. IEEE Trans. On*, vol. 36, p. 1650‑1658, sept. 2008, doi: 10.1109/TPS.2008.928715.

[54] K. Sato, K. Sugibayashi, et Y. Morimoto, « Species Differences in Percutaneous Absorption of Nicorandil », *J. Pharm. Sci.*, vol. 80, n° 2, p. 104‑107, févr. 1991, doi: 10.1002/jps.2600800203.

[55] D. C. Sauder et C. E. DeMars, « An Updated Recommendation for Multiple Comparisons », *Adv. Methods Pract. Psychol. Sci.*, vol. 2, n° 1, p. 26‑44, mars 2019, doi: 10.1177/2515245918808784.

[56] Z. Stojek, « The Electrical Double Layer and Its Structure », in *Electroanalytical Methods: Guide to Experiments and Applications*, F. Scholz, A. M. Bond, R. G. Compton, D. A. Fiedler, G. Inzelt, H. Kahlert, Š. Komorsky-Lovrić, H. Lohse, M. Lovrić, F. Marken, A. Neudeck, U. Retter, F. Scholz, et Z. Stojek, Éd., Berlin, Heidelberg: Springer, 2010, p. 3‑9. doi: 10.1007/978-3-642-02915-8_1.

[57] U. Pliquett, R. Langer, et J. C. Weaver, « Changes in the passive electrical properties of human stratum corneum due to electroporation », *Biochim. Biophys. Acta BBA - Biomembr.*, vol. 1239, n° 2, p. 111‑121, nov. 1995, doi: 10.1016/0005-2736(95)00139-T.

[58] U. F. Pliquett, G. T. Martin, et J. C. Weaver, « Kinetics of the temperature rise within human stratum corneum during electroporation and pulsed high-voltage iontophoresis », *Bioelectrochemistry Amst. Neth.*, vol. 57, n° 1, p. 65‑72, juill. 2002, doi: 10.1016/s1567-5394(01)00177-3.

[59] A. Pertovaara, T. Kauppila, et M. M. Hämäläinen, « Influence of skin temperature on heat pain threshold in humans », *Exp. Brain Res.*, vol. 107, n° 3, p. 497‑503, janv. 1996, doi: 10.1007/BF00230429.

[60] T. Forjanic *et al.*, « Electroporation-Induced Stress Response and Its Effect on Gene Electrotransfer Efficacy: In Vivo Imaging and Numerical Modeling », *IEEE Trans. Biomed. Eng.*, vol. 66, n° 9, p. 2671‑2683, sept. 2019, doi: 10.1109/TBME.2019.2894659.

[61] U. Pliquett, Ch. Gusbeth, et R. Nuccitelli, « A propagating heat wave model of skin electroporation », *J. Theor. Biol.*, vol. 251, n° 2, p. 195‑201, mars 2008, doi: 10.1016/j.jtbi.2007.11.031.

[62] S. Becker, « Transport Modeling of Skin Electroporation and the Thermal Behavior of the Stratum Corneum », *Int. J. Therm. Sci. - INT J THERM SCI*, vol. 54, janv. 2011, doi: 10.1016/j.ijthermalsci.2011.10.022.

[63] N. Pavšelj et D. Miklavčič, « Resistive heating and electropermeabilization of skin tissue during in vivo electroporation: A coupled nonlinear finite element model », *Int. J. Heat Mass Transf.*, vol. 54, n° 11, p. 2294‑2302, mai 2011, doi: 10.1016/j.ijheatmasstransfer.2011.02.035.

[64] N. Pavselj et D. Miklavcic, « A Numerical Model of Permeabilized Skin With Local Transport Regions », *IEEE Trans. Biomed. Eng.*, vol. 55, n° 7, p. 1927‑1930, juill. 2008, doi: 10.1109/TBME.2008.919730.

[65] J. Dermol-Černe et D. Miklavčič, « From Cell to Tissue Properties—Modeling Skin Electroporation With Pore and Local Transport Region Formation », *IEEE Trans. Biomed. Eng.*, 2018, doi: 10.1109/TBME.2017.2773126.

[66] Y. A. Chizmadzhev, A. V. Indenbom, P. I. Kuzmin, S. V. Galichenko, J. C. Weaver, et R. O. Potts, « Electrical Properties of Skin at Moderate Voltages: Contribution of Appendageal Macropores », *Biophys. J.*, vol. 74, n° 2, p. 843‑856, févr. 1998, doi: 10.1016/S0006-3495(98)74008-1.

[67] E. A. Leclerc, A. Huchenq, S. Kezic, G. Serre, et N. Jonca, « Mice deficient for the epidermal dermokine β and γ isoforms display transient cornification defects », *J. Cell Sci.*, vol. 127, n° 13, p. 2862-2872, juill. 2014, doi: 10.1242/jcs.144808.

[68] M. M. Martin et L. Lindqvist, « The pH dependence of fluorescein fluorescence », *J. Lumin.*, vol. 10, n° 6, p. 381-390, juill. 1975, doi: 10.1016/0022-2313(75)90003-4.

[69] D. J. Arndt-Jovin et T. M. Jovin, « Chapter 16 Fluorescence Labeling and Microscopy of DNA », in *Methods in Cell Biology*, vol. 30, D. L. Taylor et Y.-L. Wang, Éd., in Fluorescence Microscopy of Living Cells in Culture Part B. Quantitative Fluorescence Microscopy—Imaging and Spectroscopy, vol. 30. , Academic Press, 1989, p. 417-448. doi: 10.1016/S0091-679X(08)60989-9.

[70] L. Finlayson *et al.*, « Depth Penetration of Light into Skin as a Function of Wavelength from 200 to 1000 nm », *Photochem. Photobiol.*, vol. 98, n° 4, p. 974-981, 2022, doi: 10.1111/php.13550.
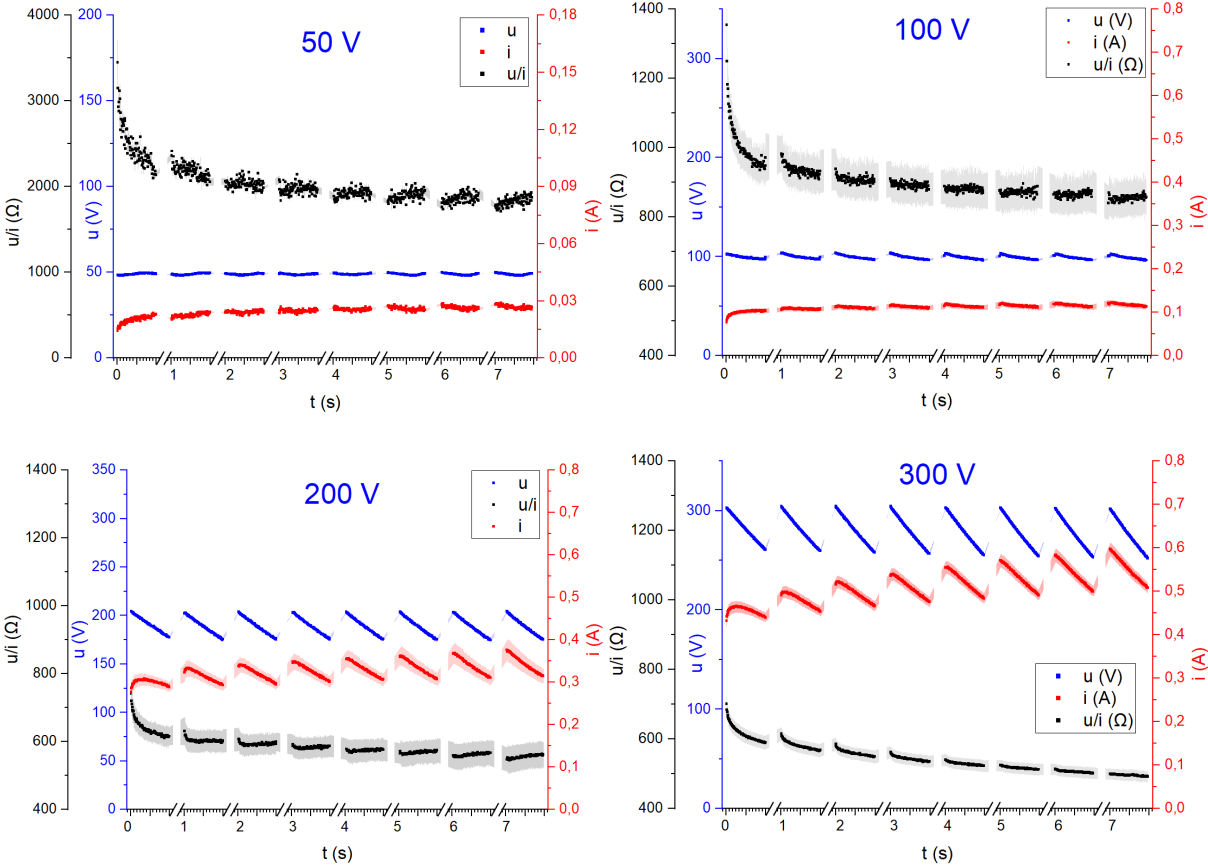
**Fig. S1.** Voltage, current and instantaneous resistance (u/i) of drug delivery setup during Pulsed Electric Fields (PEF) of voltages from 50 to 300 V. Shaded areas represent SEM. (50V,200V: n=3; 100V: n=5; 300V: n=12).
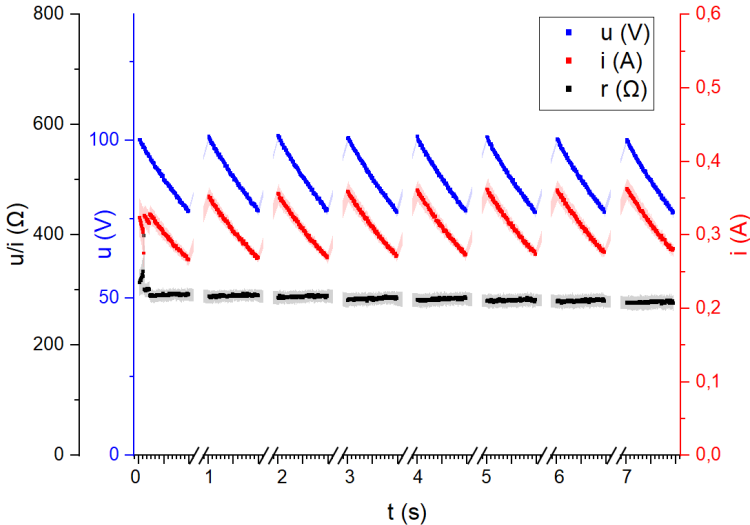

Fig. S2. Voltage and current of the system without mouse skin (only hydrogels and gauze). There was no variation of *r(t)=u(t)/i(t)* during PEF application. This showed that the resistance decrease was attributed to the skin. Shaded areas represent SEM. n=3
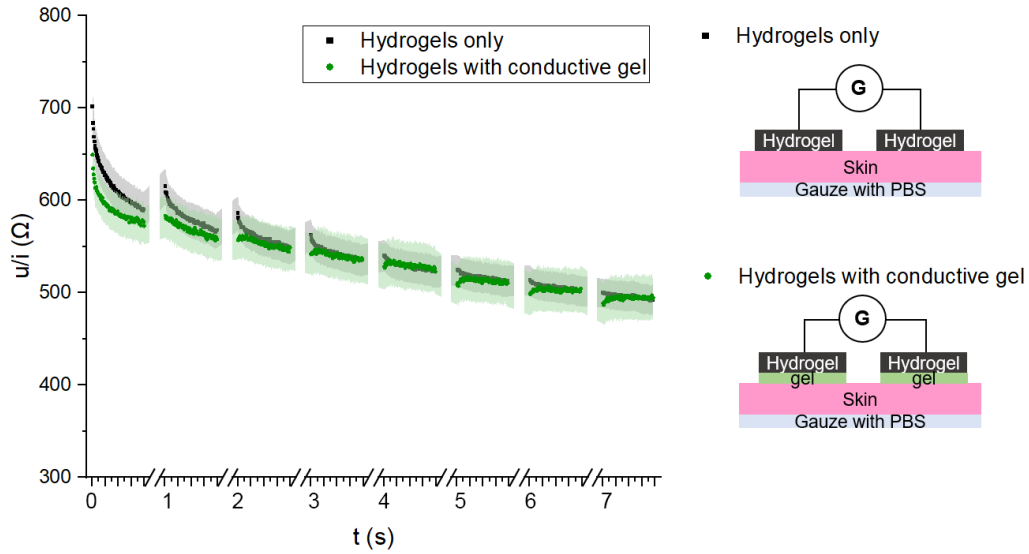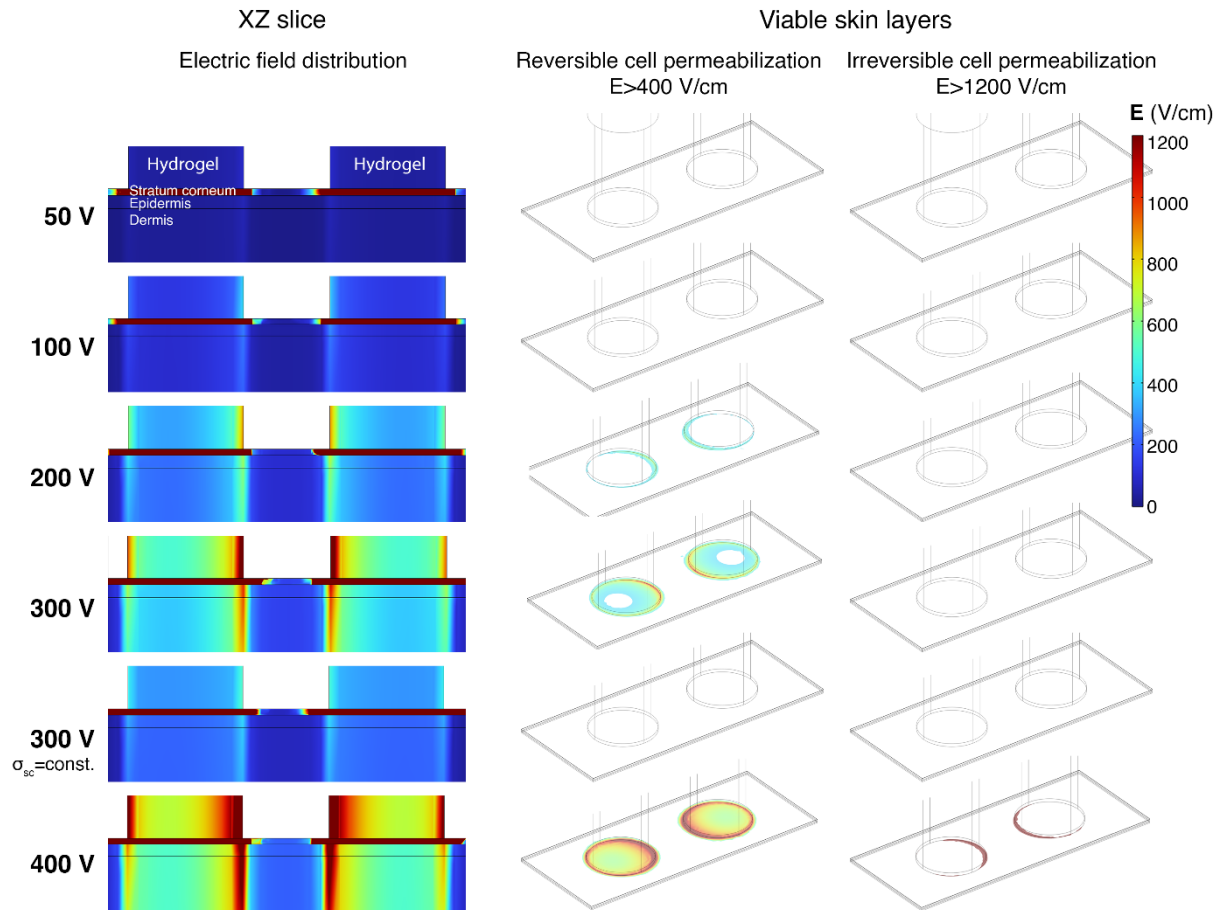
Fig. S3. Instantaneous resistance ($r(t)=u(t)/i(t)$) of electroporation system with skin and hydrogels only (black, n=12) and with skin, hydrogels and conductive gel between them (green, n=3). Adding conductive gel between the hydrogels and the skin does not improve electrical contact, therefore it is rendered unnecessary, for our configuration. Shaded areas represent SEM.
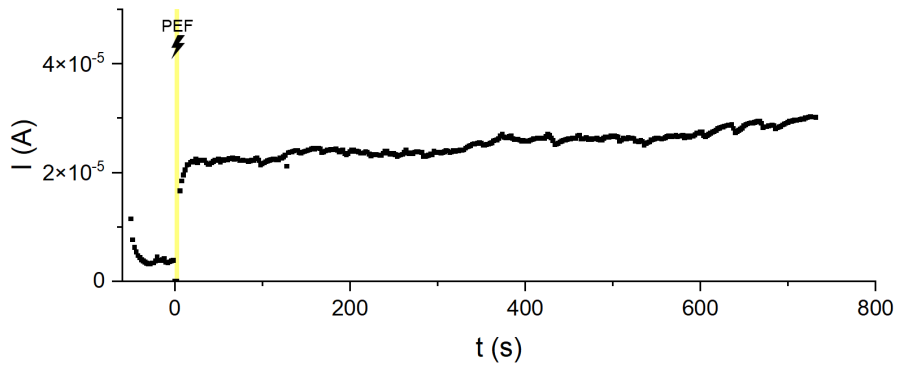

Fig. S4. Electric current resulting from the application of 1V DC, before and after PEF at 300 V. The DC resistance of the skin did not recover for up to 12 minutes. The change in the electrical properties of the skin appeared to be long-lived, or permanent, after 300 V PEF. Yellow shaded area corresponds to PEF application.
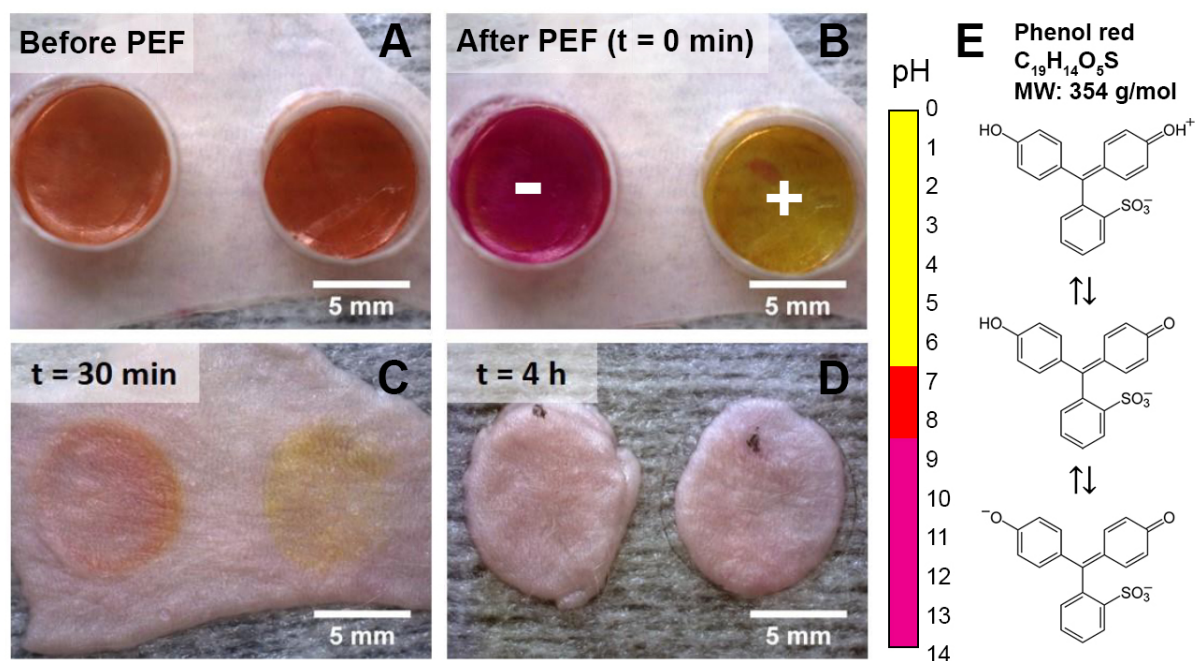
Fig. S5. Evaluation of pH changes in hydrogels and on the surface of the skin. A pH indicator, phenol red, was incorporated into two agarose hydrogels (without CNTs, to maintain their transparency), and a 300 V PEF was applied through them, on the surface of the skin. (A) Before PEF, the color of the dye was red orange, corresponding to a pH between 6.8 and 8.2. The hydrogels were buffered at pH=7.4. (B) Immediately after PEF application the color of the indicator shifted to magenta red in the negative electrode (pH>8.2) and yellow in the positive electrode (pH<6.8). (C) Phenol red was delivered into the mouse skin, under the influence of the PEF. (D) After few hours, pH changes were equilibrated, through diffusion. (E) Phenol red color scale with pH changes. The protocol for this experiment was the same as with the delivery of fluorescent molecules with the following changes: plain agarose hydrogels were used (without CNTs), no fluorophores were loaded in the hydrogels and the hydrogels were left in place for 30 minutes instead of 15, after PEF application.

XZ slice   Viable skin layers

Electric field distribution   Reversible cell permeabilization   Irreversible cell permeabilization
E>400 V/cm   E>1200 V/cm

Fig. S6. Electric field distribution on skin for PEFs from 50 to 400 V, including 300 V PEF on skin with fixed conductivity $\sigma_{SC}=5\times10^{-4}$ S/m. XZ slices of electric field distribution and areas where the electric field reaches values over 400 V/cm and over 1200 V/cm on the viable skin (under the stratum corneum).
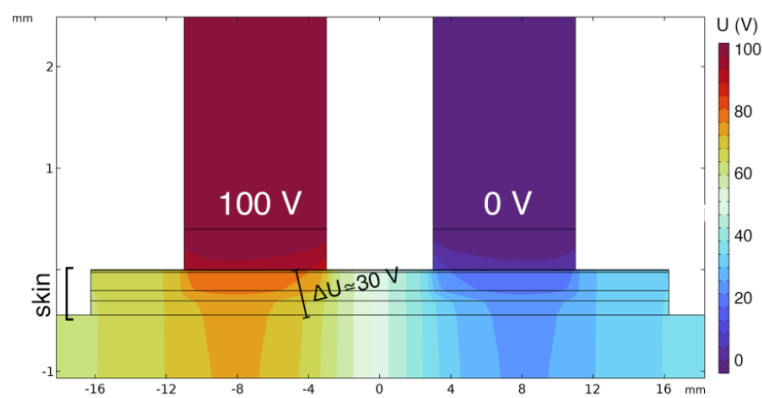
Fig. S7. Potential difference across skin for 100 V PEF. A 100 V PEF would result in an estimated potential difference of approximately 30 V across the skin. It's important to note that due to the non-uniform electric field resulting from the side-by-side electrode configuration, this estimation is approximate.
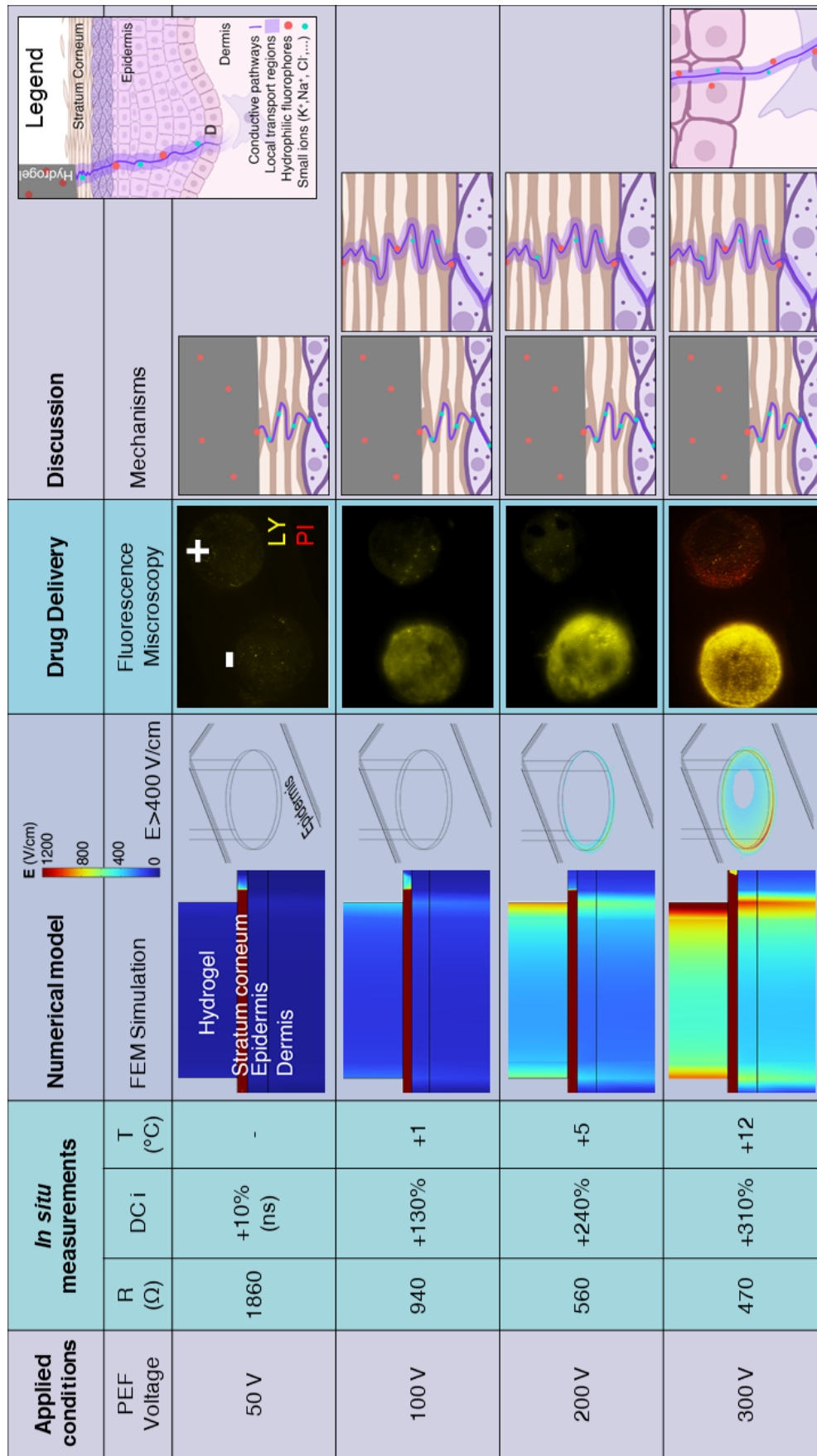
Fig. S8. Summary of experimental results on transdermal drug delivery, for applied PEFs of 50 to 300 V (8 pulses, 20 ms duration, 1 Hz). **In situ measurements.** Average resistance (U/I) during last pulse, DC current change after PEF, Temperature increase (max) during PEF. **Numerical model.** Electric field distribution on the skin, through validated, nonlinear model. XZ slices of first skin layers and areas where E>400 V/cm (approximate threshold value for cell permeabilization in tissue) on viable skin layers. **Drug delivery.** Fluorescent marking of lucifer yellow (LY) and propidium iodide (PI) on skin, after PEF. **Discussion.** Proposed mechanisms for each voltage: creation of conductive pathways, formation of local transport regions and cell permeabilization.